A new inventory of High Mountain Asia surging glaciers derived from multiple elevation datasets since the 1970s

Lei Guo[1], Jia Li[1], Amaury Dehecq[2], Zhiwei Li[1], Xin Li[3], Jianjun Zhu[1]

[1]School of Geo-science and Info-physics, Central South University, Changsha, 410083, China.
[2]Univ. Grenoble Alpes, IRD, CNRS, Grenoble INP, IGE, Grenoble, 38000, France.
[3]Institute of Tibetan Plateau Research, Chinese Academy of Sciences, Beijing, 100101, China.

Correspondence to: Jia Li (lijia20050710@csu.edu.cn)

Abstract. Glacier surging is an unusual instability of ice flow and complete inventories of surging glaciers are important for regional glacier mass balance studies and glacier dynamic studies. Glacier surge events in High Mountain Asia (HMA) are widely reported. However, the completeness of present inventories of HMA surging glaciers is constrained by the insufficient spatial and temporal coverage of glacier change observations, or by the limitations of the identification methods. In this study, we established a new inventory of HMA surging glaciers based on the glacier surface elevation changes and morphological changes over four decades. Four types of elevation sources (the KH-9 DEM, NASA DEM, COP30 DEM, and HMA DEM), three elevation change datasets, and long-term Landsat image series were utilized to assess the presence of typical surge features over two time periods (1970s-2000 and 2000-2020). A total of 890 surging and 336 probably or possibly surging glaciers were identified in HMA. Compared to the most recent inventory of surging glaciers in HMA, our inventory incorporated 253 previously unidentified surging glaciers. The number and area of surging glaciers accounted for ~2.49% (excluding glaciers smaller than 0.4 km^2) and ~16.59% of the total glacier number and glacier area in HMA, respectively. Glacier surges were found in 21 of the 22 subregions of HMA (except for the Dzhungarsky Alatau), however, the density of surging glaciers is highly uneven. They are common in the northwest subregions (e.g., Pamir and Karakoram), but scarce in the peripheral subregions. The inventory further confirmed that surge activity is more likely to occur for glaciers with a larger area, longer length, and wider elevation range. Among glaciers with similar areas, the surging ones usually have steeper slopes than non-surging ones. Besides, we found a potential relationship between surging glacier concentration and regional glacier mass balance. The subregions with slightly negative or positive mass balance hold large clusters of surging glaciers, while those with severe mass loss hold very few surging glaciers. The inventory and elevation change products of identified surging glaciers are available at: https://doi.org/10.5281/zenodo.7590838 (Guo et al., 2022).

Key words: High Mountain Asia, Surging glacier inventory, elevation change, KH-9, Digital Elevation Model (DEM)

1 Introduction

A surge is a glacier instability that translates into an abnormally fast flow over a period of a few months to years (Cogley et al., 2011). A surging glacier exhibits an active phase (surge) and a quiescent phase that may occur at quasi-periodic intervals (Jiskoot, 2011). During a glacier's surging phase, a large volume of ice mass is transported downstream at a higher-than-average speed. In the quiescent phase, a glacier returns to a slow-moving state, and gradually regains mass in upper reaches. Previous studies pointed out that surge-type glaciers only represent ~1% of total glaciers (Jiskoot, 2011; Sevestre and Benn, 2015). However, glacier surges are far more than an occasional behavior in some specific regions, such as the Alaska-Yukon (Clarke et al., 1986), Svalbard (Jiskoot et al., 2000; Farnsworth et al., 2016), and Karakoram-Pamir (Bhambri et al., 2017; Goerlich et al., 2020; Guillet et al., 2022). Glaciers in these regions have experienced heterogeneous mass loss in the past decades (Hugonnet et al., 2021). How glacier surge activities impact the regional mass balance needs further investigation and requires to identify the glacier surges firstly. In recent years, substantial efforts have been made to understand the mechanisms

of glacier surges, including the hydrological-control (Kamb, 1987; Fowler, 1987), thermal-control (Fowler et al., 2001; Murray et al., 2003), environmental factor (Hewitt, 2007; Van Wyk de Vries et al., 2022), friction state (Thøgersen et al., 2019; Beaud et al., 2021), and the unified enthalpy balance model (Sevestre and Benn, 2015; Benn et al., 2019). These theories require comprehensive validations by conducting detailed analysis on various glacier samples. To support related investigations, the distribution of surging glaciers is needed as a starting point.

Generally, a surging glacier could exhibit either one or several drastic changes, including: extreme speed-up (by a factor of 10~1000 compared to the usual flow of non-surging glaciers), distinct elevation change pattern, rapid terminus advance, and surface morphological changes (deformed medial or looped moraines, crevasses, shear margins, etc.) (Jiskoot, 2011). The identification of surging glaciers can be implemented based on the observation of the above changes, e.g., glacier surface morphology(Clarke et al., 1986; Paul, 2015; Farnsworth et al., 2016), terminus position (Copland et al., 2011; Vale et al., 2021), glacier motion (Quincey et al., 2011), or morphological-related indicators (e.g., normalized backscatter difference (Leclercq et al., 2021))). A surge-type glacier, which refers to a glacier that possibly surged prior to the observation period, is generally identified by indirect morphological evidence (without observed changes) (Goerlich et al., 2020). The visual interpretation of glacier surface morphological changes is less calculative, but fraught with uncertainty due to the snow cover or the absence of supraglacial moraine deformation (Jacquemart and Cicoira, 2022). To recognize sudden changes in glacier motion, a long-term flow velocity time series is needed (Yasuda and Furuya, 2015; Round et al., 2017). Since the quiescent phase may last for decades and the image sources for estimating the flow velocity are limited, the strong changes in glacier motion might be missed. In contrast, the recognition of a specific surface elevation change pattern is a more reliable way to identify surging glaciers, as it will be visible for many years before and after a surge (Bolch et al., 2017; Zhou et al., 2018). Accordingly, its source datasets (DEMs) can satisfy the required spatio-temporal coverage with comparatively fewer datasets. By combining observations of multiple features, the identification of surging glaciers could be more efficient and complete (Mukherjee et al., 2017; Goerlich et al., 2020; Guillet et al., 2022). However, when conducting such studies on a large spatial scale or a long temporal scale, one should select the least time-consuming but most effective identification method. In that case, it's ideal to take the long-term elevation change as a criterion and to combine this information with other observations if possible (Guillet et al., 2022).

Except for the polar regions, High Mountain Asia (HMA) is the most densely glacierized region in the world. Within the HMA range, several subregions are famous for the concentration of surging glaciers as well as the differing glacier mass balance (Hewitt, 2005; Gardelle et al., 2013; Farinotti et al., 2020). The inventories of surging or surge-like glaciers have been established for some subregions like the Karakoram (Bhambri et al., 2017), West-Kunlun (Yasuda and Furuya, 2015), Pamir (Goerlich et al., 2020) and Tien Shan (Mukherjee et al., 2017; Zhou et al., 2021). Sevestre and Benn (2015) presented the first global inventory of surging glaciers by reanalyzing historical reports from 1861 to 2013. However, it was compiled from various data sources (publications, reports, etc.) with inconsistent spatio-temporal coverage, which makes it difficult to ensure accuracy and completeness. Vale et al. (2021) identified 137 surging glaciers across HMA by detecting surge-induced terminus change and morphological changes from Landsat images from 1987 to 2019. The number is obviously underestimated, because it is smaller than the numbers of previous subregional inventories (Bhambri et al., 2017; Goerlich et al., 2020), i.e. not all glaciers that surge do also advance. Guillet et al. (2022) presented a new surging glacier inventory of HMA by identifying multiple glacier change features. In total 666 surging glaciers were identified across HMA. However, the glacier change observation period is shorter than two decades (2000-2018), and therefore some surging glaciers with relatively long-repetition cycles may be missed.

In this study, we aimed to build a new inventory to include more surging glaciers within HMA based on glacier surface elevation changes observations over four decades. A workflow was developed to obtain the historical glacier surface elevation change from multiple DEMs, including the KH-9 DEM (1970s), NASA DEM (2000), COP30 DEM (2011-2014), HMA DEM (2002-late 2016), and previously published elevation change datasets. The preliminary identified surging glaciers were divided

into three classes of confidence in surge detection. After that, the elevation change based inventory was further completed and corrected by the identification of morphological changes in a long-term time series of Landsat images (1986-2021). Based on the present inventory, the distribution and geometric characteristics of surging glaciers within HMA were statistically analyzed, in order to demonstrate their spatial heterogeneity and geometrical difference from the normal glaciers.

2 Study region

High Mountain Asia consists of the Qinghai-Tibet Plateau and its surrounding regions, including the Karakoram, Pamir, Himalayas, and Tien Shan. According to the updated Glacier Area Mapping for Discharge from the Asian Mountains (GAMDAM2) glacier inventory, HMA hosts 131819 glaciers, covering a total area of ~99817 km^2 (Sakai, 2019). The Hindu Kush Himalayan Monitoring and Assessment Programme (HiMAP) divided HMA into 22 subregions (Fig. 4) (Bolch et al., 2019). Different subregions are influenced by different climate regimes, such as the South Asia monsoon, the East Asia monsoons, and the westerlies (Bolch et al., 2012; Maussion et al., 2014). Glacier elevation changes across HMA were found to be heterogeneous in the past decades (Gardelle et al., 2013; Brun et al., 2017; Shean et al., 2020). In particular, glaciers in the Pamir-Karakoram-West Kunlun region had slightly positive or close to zero changes (Hewitt, 2005; Zhou et al., 2017; Farinotti et al., 2020), while those in the Eastern Himalayas, Nyainqentanglha and Hengduan Shan mountain ranges experienced substantial ice loss (Maurer et al., 2019).

3 Datasets

3.1 Elevation Data

The NASA DEM is mainly reprocessed from the C-band SRTM (Shuttle Radar Topography Mission) images. Among the current global DEMs, the NASA DEM has the shortest source data acquisition period (~11/02/2000~22/02/2000) (Farr et al., 2007). Based on an improved production flow, the NASA DEM has a better performance than the earlier SRTM void-free product in most regions (Crippen et al., 2016). The NASA DEM serves as the reference elevation source because its acquisition time, 2000, is suitable to divide the elevation change observations into before and after the 21st century with a moderate time span (one or two decades). Each tile of the product has an extent of 1°× 1° and a pixel spacing of 1 arc-second (see Fig. 1a). In total 313 tiles were downloaded from NASA LP DAAC (https://e4ftl01.cr.usgs.gov/MEASURES/NASADEM_HGT.001/). Another global DEM we utilized is the newly released Copernicus DEM GLO-30-DGED (i.e., COP30 DEM). The COP30 DEM was edited from the delicate WorldDEM™, which was generated based on the TanDEM-X mission. The global RMSE of the COP30 DEM is ±1.68 m (AIRBUS, 2020). Several studies have pointed out that this DEM is the most reliable open-access DEM to date (Purinton and Bookhagen, 2021; Guth and Geoffroy, 2021). The source images of the COP30 DEM were mostly acquired between 2011 and 2014, and therefore the COP30 DEM is suitable for representing the surface elevation in the 2010s. Like the NASA DEM, the COP30 DEM has a pixel spacing of 1 arcsecond. Each tile of the product has an extent of 1°× 1°. In total 313 tiles were downloaded through ESA Panda (https://panda.copernicus.eu/web/cds-catalogue/panda).

The High Mountain Asia 8-meter DEM (HMA DEM) was also utilized in this study. The HMA DEM was generated from very high-resolution commercial optical satellite stereo images, including WorldView-1/2/3, GeoEye-1, and Quickbird-2 (Shean et al., 2020), through an automated photogrammetry workflow that is integrated with multiple error-control processes (Shean et al., 2016). This DEM was originally produced for the mass balance estimation of HMA glaciers, so it covered most of the glacierized regions in HMA. In total 3598 DEM tiles were downloaded from the National Snow and Ice Data Center (https://nsidc.org/data/HMA_DEM8m_MOS/versions/1). About 95% of them were acquired between 2010 and 2016 (Fig. 1b). Due to the data voids and inconsistent acquisition time, the HMA DEM was taken as a supplementary elevation source to increase the observations in the 2010s.

The Hexagon KeyHole-9 (KH-9) imagery was acquired in the 1970s. It is one of the earliest near-global satellite stereo image sources. The KH-9 imagery is characterized by a spatial resolution of 6-9 m, a wide coverage (130 km x 260 km), and a 70% forward overlap (Surazakov and Aizen, 2010). Many studies have utilized this imagery to estimate historical glacier surface elevation (Holzer et al., 2015; Zhou et al., 2017; Maurer et al., 2019). The KH-9 DEMs used in this study were generated through the automated ASPy pipeline (Dehecq et al., 2020). The methodology, validated in the European Alps and Alaska, achieved a vertical accuracy of ~5m (68% confidence level). For more details on the method of KH-9 DEM generation, please refer to Dehecq et al. (2020). In total 238 DEMs with a resolution of 48 m were generated from the KH-9 images acquired between 1973 and 1980 (see Fig. 1c). The KH-9 DEMs were utilized to represent the glacier surface elevation in the 1970s. Several newly published elevation change datasets were also collected to include the most recent surges (Brun et al., 2017; Shean et al., 2020; Hugonnet et al., 2021). We mainly used the elevation change results presented by Hugonnet et al. (2021) to extend the observation period to 2020, which has a resolution of 100 m and a temporal interval of 5 years. Through the inter-comparison of the multiple elevation change results, the gross errors or false signals in the elevation change patterns could be easily detected and removed.

3.2 Optical Satellite Images

In order to assist in the identification of surging glaciers, we also identified morphological changes associated with surges in multi-temporal optical satellite images. We mainly relied on the 1986-2021 Landsat imagery to capture morphological changes. We acknowledge that due to the 30 m spatial resolution, not all details of a changed glacier surface are visible. We downloaded the false-color composited Landsatlook images with 30m resolution (geo-referenced) that have good brightness contrast over snow/ice areas from the USGS (https://earthexplorer.usgs.gov). The images were pre-selected to satisfy the requirement of cloud cover (<10%). In total, 7843 Landsatlook images in 148 frames were used (see Fig. 1d). We also utilized the very high-resolution (VHR) images (Google/ESRI/Bing, etc.) as complements for surging feature identification. The fine resolution of these images allows us to visually check the possible morphological features caused by past surges.

3.3 Glacier inventory

In this study, we used the GAMDAM2 glacier inventory (Sakai, 2019) as a template for the inventory of surging glaciers, rather than the Randolph Glacier Inventory V6.0 (RGI6.0) (RGI Consortium, 2017). The GAMDAM glacier inventory has included many small glaciers that are missed in RGI6.0, and provides a more accurate glacier extent by also excluding rock outcrop rocks, seasonal snow, and shaded areas (Nuimura et al., 2015). Since the GAMDAM2 inventory only contains the glacier polygon vectors, we calculated the geometric and topographic attributes for each glacier in a way similar to that of RGI6.0. The maximum glacier centreline was calculated through the Open Global Glacier Model (OGGM) (Maussion et al., 2019). The attributes were used to interpret the geometric characteristics of surging glaciers.

4 Methodology

4.1 Estimation of glacier surface elevation change

The four kinds of DEMs have different coordinate references, vertical references, and data formats. Firstly, all DEMs were converted to float GeoTiff format. For datasets with quality files (the NASA DEM and the COP30 DEM), the DEMs were preprocessed to mask out the pixels of low quality. The poor pixels in the COP30 DEM tile were determined through the attached height error map (with values larger than 2.5 m) and water body map (with values not equal to zero). The NASA DEM was directly masked with the attached water mask file. Subsequently, the coordinate system, map projection, and vertical reference of all DEMs tiles were unified as the WGS84 coordinate system, HMA Albers Equal Area projection (Shean et al., 2020), and WGS84 ellipsoid. The glacier surface elevation changes during 2000-2010s were derived by subtracting the NASA

DEM from the COP30 DEM and HMA DEM, and those during 1970s-2000 were derived by subtracting the KH-9 DEM from the NASA DEM.

An automated DEM differencing workflow for large-scale glacier surface elevation change estimation was developed based on the *demcoreg* package presented by Shean et al. (2019). The workflow integrated multiple DEM co-registration approaches, such as the polynomial fit of tilt error, and other adaptive outlier removal approaches that were operated based on the observations over stable regions. Hence, a mask that excluded the water bodies and glacierized regions was generated in advance. Before differencing, the two DEMs need to be co-registered, because a small geolocation shift can result in considerable elevation change errors in high-mountain regions. The efficient analytical DEM co-registration method presented by Nuth and Kääb (2011) was used to eliminate the relative geolocation shift (horizontal and vertical) between DEMs. This method assumes the geolocation shift vectors of all DEM pixels are identical. However, for the global DEM products like the NASA DEM and the COP30 DEM, a DEM tile was usually merged from multiple DEM patches, and the geolocation shift vectors at different parts of the DEM tile may be different. In view of this problem, we developed a block-wise version of the analytical DEM co-registration method to reduce the impacts of geolocation accuracy anisotropy of a DEM tile. Each DEM tile was divided into m×n blocks, and the DEM shifts were estimated for each block. Then, the m×n groups of shift parameters were merged into one group of shift parameters through a cubic interpolation. Technically, the estimated shift parameters become increasingly representative as the block size decreases. However, the fitting of shift parameters requires a certain number of samples. The final block size was set to 300×300 pixels to reach the best balance between the representativeness and estimation accuracy of the shift parameters. Besides, we found that the block-wise co-registration method could result in wrong fitting of shift parameters over flat regions. To deal with this, a threshold of mean slope (10°) was set to classify the DEMs into the flat and the hilly categories, and the original global co-registration method (Nuth and Kääb, 2011) was applied to the flat ones.

Due to the residual orbital error of satellite images, the elevation difference maps often showed planimetric trends. This type of systematic error was fitted as a universal surface trend using a quadratic polynomial model based on the observations in stable regions, and then was removed from the elevation difference tile (Li et al., 2017). Besides, due to the jitter of the SAR antenna and optical mapping camera, the elevation difference maps often showed stripes (i.e., band-like artifacts) (Yamazaki et al., 2017). To eliminate the stripes, the elevation difference map was converted to the frequency domain through a Fast-Fourier-Transform method. Since the cyclic values have a high frequency in the power spectral density map, a threshold of frequency was set to separate the stripes components from the normal elevation differences. The de-stripping was completed after the backward transformation. Finally, the outliers of elevation difference maps were reduced through the 3-sigma threshold criterion.

The radar penetration into glacier surface can result in biases of elevation change estimation, which could be several to dozens of meters, and potentially lead to false values. We adopted a two-step procedure to reduce the radar penetration bias in the final elevation change results. First, we used the DEM differencing workflow mentioned above to subtract the NASA DEM from the SRTM-X DEM. The elevation differences over glacierized area were regarded as the penetration difference between X-bands and C-bands. Secondly, we fitted a 3rd polynomial function between the glacial dH and altitude, which was deemed as the penetration depth – altitude relationship. Then, the radar penetration biases were removed from the COP30 DEM related results by taking the glacier elevation as input for the function. For the dH results calculated by differencing the NASA DEM and optical DEMs (e.g. the HMA and KH-9 DEM), the penetration difference of X- and C- bands was multiplied by 2 to represent the absolute penetration depth of C-band (Abdel Jaber et al., 2019; Fan et al., 2022) and then removed from the related results.

Finally, three elevation change maps were calculated: the COP30 DEM – NASA DEM, the HMA DEM – NASA DEM, and the NASA DEM – KH-9 DEM. The first two elevation change maps were combined with the three elevation change datasets for surging glacier identification during the period 2000-2020, and the last one during the period 1970s-2000. In total, our

elevation change observations covered ~92% of the total glacier area within HMA in 2000-2020, and ~77% in 1970s-2000. Gaps in observations were mainly due to: 1) data voids and incomplete coverage of the original DEMs tile, which was the main cause for the KH-9 DEMs and HMA DEM related results; 2) gross error removal during the elevation change calculations, which led to the scattered holes in the COP30 DEM related results.

4.2 Surging glacier identification

The identification of surging glaciers in this study was divided into three steps. First, we generated a raw inventory of surging glaciers through the qualitative interpretation of multi-temporal elevation changes. Then, the visual identification of morphological changes was carried out for the identified surging and surge-like glaciers. This procedure can further confirm the surges or correct the false identifications based on glacier elevation changes (Guillet et al., 2022). The identified results were re-checked by careful inspection on VHR images, and by comparing with existing surging glacier inventory. Also, the surging tributaries were separated from the non-surging glacier trunk at this step.

4.2.1 Identification through elevation changes

In general, a typical glacier surge cycle can be divided into three phases (Jiskoot, 2011): 1) the build-up phase, characterized by remarkable thickening in the upper reaches; 2) the active phase, characterized by remarkable thinning in the upper reaches and thickening in the lower reaches; 3) the post-surge phase, characterized by strong down-wasting in the lower reaches. The classical method of identifying surging glaciers is to recognize the combination of marked upper thinning and lower thickening in the longitudinal direction. However, to distinguish the surging glaciers in the build-up or post-surge phase, careful comparison with surrounding glaciers is required, which is difficult to be carried out with a mathematical index. In this study, we established a three-class indicator to distinguish the surge possibility through the visual interpretation of glacier elevation change patterns:

I) “verified”:
- a) obvious thickening in lower reaches (e.g. +30 m);
- b) contrasting upper-thinning (e.g. +20 m) and lower-thickening (e.g. +20 m);
- c) contrasting upper-thickening (e.g. +20 m) and lower-thinning (e.g. -30 m);
- d) severe thinning in the lower reaches (two times stronger than that of the normal glaciers, or comparable to the ablation of adjacent “verified” surging glaciers);

II) “probable”:
- a) moderate upper thinning (e.g. -15m) and lower thickening (e.g. +15m);
- b) only moderate thickening in the middle reaches (e.g. +15m);

III) “possible”:
- a) only moderate thickening at the terminus (e.g. +15m);
- b) only strong thinning in the lower reaches (one time stronger than adjacent normal glaciers).

Note that, the specific values of elevation change mentioned above were for information only. Because of the diversity in the regional elevation change patterns under different climate or topographic conditions, the thresholds may vary spatially.

The identification of surging glaciers was conducted separately in the two observation periods (1970s-2000 and 2000-2020). The sub-inventory covering the period 1970s-2000 was generated based on the dH results of the NASA DEM – KH-9 DEM. For the sub-inventory covering the period 2000-2020, its dH datasets contain the COP30 DEM – NASADEM, the HMA DEM – NASADEM, and three previously published elevation change datasets (Brun et al., 2017; Shean et al., 2020; Hugonnet et al., 2021). Within each observation period, each glacier will be labeled with its possibility level of surging and elevation change pattern in the attribute table. For example, the label “I-c” means this glacier was classified as a “verified” surging glacier

because contrasting upper-thickening and lower-thinning patterns were observed in the corresponding period. Figure 2 shows an example of surging glacier identification result.

4.2.2 Identification through morphological changes

Long-term Landsat images (acquired between 1986 and 2021) were utilized to investigate the morphological changes of the three types of potential surging glaciers identified from elevation change. With each Landsat image acquisition frame, all Landsatlook images of different dates (acquired from 1986 to 2021) were merged into an animated time-series image. Based on the animated image, we are able to easily identify the morphological changes. Due to the moderate resolution of Landsat images, only three types of feature changes were utilized as criteria for identifying glacier surges: terminus position change, looped moraine changes, and medial moraine changes. Similarly, we assigned a two-level index to each morphological change to indicate our confidence in the identification, which was defined as follows:

1) terminus advance:
    I): obvious terminus advancing (e.g. over 500 m);
    II): slight terminus advancing (e.g. 0~500 m);
2) looped/medial moraine change:
    I): fast formation/vanishment of the looped moraine, or obvious distortion of the medial moraine;
    II): slow formation or vanishment of the looped moraine, or slight shape changes of existing looped moraine, or slight distortion of the medial moraine.

Each of the three kinds of morphological changes was individually qualified and labeled in the attribute table.

4.2.3 Generation of surging glacier inventory

Through the above identification steps, in total five indicators were compiled to describe the changes of possible surging glaciers. The two sub-inventories of dH identified results were merged firstly following the principle of possibility, i.e., if a glacier was identified as a surging glacier in both periods but associated with different indicators, its indicator in the final inventory was taken from the indicator having a higher possibility. The possibility of indicators follows the order: “verified” > “probable” > “possible”. For example, a glacier was identified as a “verified” surging glacier in the period 1970s-2000, and was identified as a “probable” surging glacier in the period 2000-2010s, then it was qualified as a “verified” surging glacier. After that, the merged dH indicators were further compared with the morphological indicators to determine the final indicator of surge possibility. The “probable” or “possible” class was changed to a class with higher possibility (e.g., from “probable” to “verified”) only if an “I” kind of morphological change was found.

We think the advancing glaciers usually have such features: 1) only thickened in a small area at the terminus, without contrasting upper thinning; 2) the advancing distance is relatively short (Lv et al., 2019, 2020; Goerlich et al., 2020). These features are corresponding to the “III-a” type of elevation change, and the “II” type of terminus advance. Therefore, if a glacier only shows these two kinds of changes, it will be qualified as an advancing glacier, rather than a surging glacier.

For glacier complex in which a tributary surged but the main trunk did not show any features of a surge, such as the Biafo glacier, Fedchenko Glacier, and Panmah Glacier (Hewitt, 2007; Goerlich et al., 2020; Bhambri et al., 2022), it’s necessary to separate the surging tributary from the trunk. A tributary will be considered as an individual surging glacier if it has the following features. Firstly, the transition of contrasting elevation change is located in this tributary. Secondly, the mass contributed by this tributary to the glacier trunk is relatively small. Then we manually edited the outline to separate the tributary from the glacier complex. This kind of surge was also marked by the attribute of “trib_surge”.

In the final step, we inspected the identified surging glaciers on VHR imagery. The inspection aimed to remove the wrong identification due to some false signals, such as the severe lower-thinning in a lake-terminating glacier and remarkable surface

heightening caused by nearby landslides. We also refined our inventory after careful comparison with inventories presented by Guillet et al. (2022), Goerlich et al. (2020), and Bhambri et al. (2017).

5 Results

5.1 Identified surging glaciers

A total of 1226 surge-related glaciers across the HMA were identified based on the elevation changes and morphological changes. The identified surge-related glaciers consisted of 890 'verified' surging ones, 208 'probable' ones, and 128 'possible' ones. A total of 175 surging tributaries were identified in 86 glacier complexes. When merging the identification results of the two periods, we found that a considerable proportion of identified surging glaciers were simultaneously recognized in both periods. This makes our inventory more reliable since a surging glacier could exhibit different kinds of changes in different periods. For example, 26 probable and 51 possible surging glaciers identified during 2000-2020 turned out to be "verified" surging glaciers during 1970s-2000. Meanwhile, 60 "probable" and 21 "possible" surging glaciers identified during 1970s-2000 turned out to be 'verified' surging glaciers during 2000-2020. Thanks to the almost complete coverage of elevation change observations, we were able to classify almost all glaciers in HMA. Table 1 shows the number of surging glaciers identified from two periods of elevation changes and morphological changes. Due to the incomplete coverage of KH-9 DEMs, 103 identified surging glaciers have no observations during the period 1970s-2000. The data voids in KH-9 DEMs may be one of the reasons why fewer surging glaciers were identified in this period. In the following text, the "probable" and "possible" classes were deemed as surge-like glaciers, and only the "verified" surging glaciers were used for analysis and comparison throughout the rest of this study.

5.2 Distribution of surging glaciers

Surging glaciers were identified in 21 subregions of HMA (except for the Dzhungarsky Alatau), however, the density of identified surging glaciers is far from even (Fig. 3). Glacier surges are common in the northwest regions, sporadic in the inner regions, and scarce in the peripheral regions. Figure 4 and Table 2 show the ratios of surging glacier number and area in each subregion. Considering the area of the smallest identified surging glacier is 0.42 km^2, we only took the glaciers larger than 0.40 km^2 in the glacier number related ratio. When conducting statistical analysis, the surge-like glaciers were excluded from the dataset, and a surging tributary was regarded as an individual glacier. The number (890) and area (16556.42 km^2) of identified surging glaciers accounted for ~2.49% and ~16.59% of the total glacier number and glacier area in HMA, respectively.

Among the 22 subregions, the Karakoram is the largest cluster of surging glaciers. In total 354 surging and 128 surge-like glaciers were identified in the Karakoram. The number and area of verified surging glaciers in the Karakoram accounted for 39.80% and 47.90% of the total identified surging glaciers within HMA. We found more than half of the tributary surges (101) occurred in the Karakoram, where large glaciers are much more developed than in other regions. In the Karakoram, although surging glaciers have only accounted for 8.59% of the total glacier number, their area occupied 39.48% of the total glacierized area. The Pamirs, composed of the Eastern Pamir, Western Pamir, and Pamir Alay, hosts 249 surging glaciers and 128 surge-like glaciers. About 27.74% of the glacier area in the Eastern and Western Pamir belongs to surging glaciers. We also found 28 surging tributaries in 15 glacier complexes in the Pamirs. Surging glaciers are also common in the Western Kunlun. In total 82 surging and 47 surge-like glaciers were identified in the West Kunlun, and the area of surging glaciers accounted for 30.48% of the total glacier area. The Central Tien Shan has the fourth-largest surging glacier area. In total 59 surging glaciers were identified in the Central Tien Shan, which covered 12.93% of the total glacier area. The Karakoram, Pamirs, West Kunlun, and Central Tien Shan host ~83% of the surging glaciers across HMA. Figure 5 shows the distribution of identified surging and surge-like glaciers in these four regions.

Within interior HMA subregions (including the Tibetan Interior Mountains, Eastern Kunlun Shan, and Tanggula Shan), the number of identified surging glaciers represents less than 2% of the total but the area accounted for nearly 15% of the total glacier area. Surging glaciers in these regions are generally gathered in a few watersheds. Similar localized surging glacier clusters were also found in the Nyainqentanglha, Northern, and Western Tien Shan, and Central Himalaya, but the corresponding area ratios are much lower. In these regions, our inventory covered dozens of surging glaciers, which were rarely reported before. Figure 6 shows some samples of identified surging glaciers in these regions.

5.3 Geometric characteristics of surging glaciers

In this part, only the surging glaciers and non-surging- glaciers are taken for analysis. The surge-like glaciers are not included. All glacier samples in the surging and non-surging classes are larger than 0.40 km^2.

We divided all glaciers into 9 classes according to their area, and calculated the ratios of surging glacier number and area in each class. As shown in Figure 7 and Table 3, surging glaciers were found in all classes. Both the ratios of surging glacier area and number became increasingly high as the glacier size increased, except for the last class. Surging glaciers with an area of 1~50 km^2 occupy 82% of all surging glaciers. For the three classes in which glaciers are larger than 50 km^2, the ratios of surging glaciers area and number were about 52% and 54%, respectively. In particular, 2 of 6 very large glaciers (the Siachen glacier and the Hispar glacier) surged during our observation periods.

When comparing the geometric characteristics of the surging glaciers and non-surging glaciers, we selected samples in the following way: for each surging glacier, we selected 10 non-surging glacier samples that have the closest area; and then we randomly sampled 3 out of the 10 selected non-surging glaciers. This is to minimize the discrepancy resulted from the sample differences. There are two reasons for doing so. First, the gap between the sample numbers is huge (~35000 non-surging vs. 890 surging). Second, a high proportion of non-surging glaciers are very small glaciers. The final selected 890×3 non-surging glaciers formed the reference group.

We first analyzed the distribution of surging glacier number and area in eight orientations. As shown in Fig. 8, both the number and area of glaciers facing the north are the largest, and then followed by those facing the northwest and northeast. The distribution of the glacier orientation in the reference group was different from that of the non-surging glaciers, which confirmed the statistical analysis would be affected by sample differences. The number of surging glaciers facing the north accounted for ~30.1% of the total surging glacier number, and their area accounted for ~27.8% of all surging glacier area. The number and area ratios of surging glaciers facing the north are obviously higher than that of the non-surging glaciers facing north, while the number and area ratios of surging glaciers facing northwest are obviously lower than that of the non-surging glaciers facing northwest. Meanwhile, the area ratio of surging glaciers facing northeast is considerably higher than the number ratio, but for surging glaciers facing northwest and southwest, the situation is opposite.

Figure 9 illustrates the comparisons between the basic geometric properties of surging and non-surging glaciers. The sampling strategy mentioned above was also utilized here. If we directly compare the surging glaciers with all non-surging glaciers, we will find that surging glaciers generally have a larger area, wider elevation range (i.e., the highest glacier surface elevation minus the lowest), and longer flow line (Fig 9a-c). Taking the median values as the candidates, the quantitative comparisons are 7.3 km^2 (surging) vs. 0.87 km^2 (non-surging) for glacier area, 1534 m vs. 642 m for elevation range, and 6695 m vs. 1854 m for maximum glacier length, respectively. In terms of mean surface slope and median elevation, the values of the surging glaciers are less spread out than the non-surging glaciers. However, the median values of the two kinds of glaciers are very close (see Figures 9d and 9e). If we took the non-surging glaciers in the reference group for comparison, the discrepancies between the two kinds of groups on these geometric properties became much more different. As shown in Figure 9a, the similar boxplots of the reference group and surging glacier samples proved that our sampling strategy has successfully re-organized the non-surging glacier samples for comparisons. The gaps between the surging and non-surging glaciers (reference group) in the glacier area (7.3 km^2 vs. 7.0 km^2), elevation range (1534 m vs. 1180 m), and glacier length (6695 m vs. 5560 m), are much

smaller. More importantly, the mean slope of the glaciers in the reference group becomes smaller than that of the surging glaciers.

The correlation between different glacier geometric properties was analyzed through the bivariate scatterplots (see Figure 10). Among the glacier area, glacier length, and glacier surface elevation range, any two of them have an apparent positive correlation. The glacier mean slope has a moderate correlation with glacier area, length, and elevation range as they are auto-correlated. By contrast, glacier median elevation has little correlation with these parameters. The correlation of any two geometric properties makes little difference between surging and non-surging glaciers.

6 Discussion

6.1 Uncertainty analysis

The reliability of surging glacier identification is directly related to the accuracy of glacier surface elevation change. Assuming the uncertainties in surface elevation change are similar over glacierized areas and stable areas, we evaluated the glacier elevation change uncertainties based on elevation change observations in stable areas, whose true values are zeros. Meanwhile, the uncertainties in the radar penetration calculation were also considered through the error propagation law. The normalized median absolute deviation (NMAD) is less sensitive to outliers and can be deemed as a better proxy of uncertainty in dH than the standard deviation (Höhle and Höhle, 2009). Hence, the NMAD was used to denote the uncertainty of individual glacier surface elevation change tile (Li et al., 2017). Figure 11 shows the NMAD of elevation change observations in stable areas within each DEM differencing tiles, which were used for the co-registration and biases removal during the glacier elevation change estimation. Due to large distortions in the KH-9 images, the NASADEM – KH-9 DEM results had the highest uncertainties. Benefiting from the advantages of bistatic SAR image pairs, the COP30 DEM has high quality, and the COP30 DEM related results had the lowest uncertainties. The HMA DEM related results had moderate uncertainties. The average NMAD of all DEM differencing tiles was smaller than 5 m. Significant elevation errors usually occurred in highly rugged regions such as crests and horns. The terrain of glacier surface is relatively gentle, and therefore the uncertainties of glacier surface elevation changes should be lower than the estimated values over the area where surges occur. The head of glaciers usually includes very steep faces and has a lot of uncertainties, but it does not matter too much for this study. In general, the uncertainties of our elevation change results are well-controlled. Compared with the typical surface elevation change resulting from a glacier surge (tens to hundreds of meters), the magnitudes of uncertainties are very small.

Similar to previous studies (Sevestre and Benn, 2015; Goerlich et al., 2020), the surging glacier identification in this study was completed through a manual qualitative interpretation. It's difficult to provide a quantitative index to represent the uncertainty of surge identification. However, the four-class indicator of surge likelihood could aid that to a degree.

6.2 Characteristics of surging glaciers

The direct comparisons between geometric characteristics of surging and non-surging glaciers manifest that surge activity is more likely to occur in the glacier with a larger area, wider elevation range, and longer length (Fig. 9). Previous studies also reported this phenomenon (Barrand and Murray, 2006; Jiskoot, 2011; Sevestre and Benn, 2015; Mukherjee et al., 2017; Guillet et al., 2022). Larger area, wider elevation range, and longer length mean a larger glacier scale and more mass storage. Surge is a self-balancing process of a glacier to regulate its internal instability of thermal or hydrologic conditions which needs enough mass storage. In this case, about 97% of the surging glacier has an area larger than 1 km^2. For glaciers larger than 10 km^2, surge becomes a quite common behavior (with a number ratio higher than 20%), rather than an accidental behavior (see Fig.7).

In terms of mean surface slope, we could not observe a statistically significant difference in the median value of the surging and non-surging glaciers, although the surging glaciers have a more concentrated value range (Fig 9d and Figure 10, 3rd row,

1st column). After minimizing this kind of bias, we observed an obviously higher mean slope of surging glaciers in the comparison with the reference group. Several studies have demonstrated that the surging glacier tends to have a shallower slope (Jiskoot et al., 2000; Guillet et al., 2022). However, here we reasonably argue that this rule was concluded from an unbalanced comparison, as non-surging glaciers have a higher proportion of small glaciers than surging glaciers. Meanwhile, the inverse relationship between the glacier slope and length (Clarke, 1991; Sevestre and Benn, 2015) may not apply to very small glaciers (i.e. smaller than 1 km^2). As shown in Fig. 9d and Fig. 10, among the non-surging glaciers, the small ones occupy a high proportion and their mean slope presents strong variability. Regarding this, we can conclude that steeper glaciers are more likely to surge when the comparison is restricted to similar areas. As for the glacier median elevation, since it is almost irrelevant to the glacier area, glacier length, glacier elevation range, and glacier mean slope (see Fig. 10), it can be deemed as an irregular glacier index. However, among glaciers that have similar areas, steeper glaciers generally have a lower median elevation. That's why the median elevation of surging glaciers is slightly smaller than that of non-surging glaciers (Fig. 9e).

These comparisons could now lead to a conclusion as follows: the surging glaciers are generally longer, and have a larger elevation range than non-surging glaciers, since they have more mass storage. However, when glaciers are similar in area, a steeper surface slope is more likely to lead to surge.

Besides, our results highlight that the ratio distribution of surging glaciers in eight aspects is slightly different from that of non-surging glaciers (see Fig. 8). Overall, the ratio of surging glaciers is relatively higher than the non-surging glaciers in the north and northeast directions, but lower in the northwest direction. It is generally known that glaciers facing north are more developed in HMA. Due to the orientation of the mountains, most of the large glaciers flow toward north and northeast. Besides, the area-to-number ratio of surging glaciers is much larger than non-surging glaciers in the northeast orientation, but smaller in the northwest orientation. This is true for the Karakoram, Pamirs, and West Kunlun Shan, the three largest clusters of surging glaciers, indicating that large northeast-facing glaciers have a higher chance to be surging glaciers. Accordingly, the surging glaciers facing north and northeast have a higher area ratio than that facing the northwest.

The spatial distribution of surging glaciers in HMA presents a strong heterogeneity. About 83% of identified surging glaciers were located in the northwest region including the Central Tien Shan, Pamirs, Karakoram, and West Kunlun, and their area occupied about 87% of the total identified surging glacier area (see Fig. 4 and Table 2). As discussed above, larger glaciers are more likely to surge. The northwest regions generally hold more large glaciers and therefore hold more surging glaciers. In other subregions, large glaciers are usually concentrated in some great ice fields, such as the Geladandong, Puruogangri, and Xinqingfeng. Accordingly, surging glaciers in these subregions are usually clustered in several watersheds.

Several studies have pointed out that glacier surge activities have little impact on the glacier mass balance (Gardelle et al., 2013; Bolch et al., 2017; Guillet et al., 2022). However, glacier mass balance may also affect the occurrence of glacier surges. Copland et al. (2011) concluded that the increase of glacier surges in the Karakoram could be related to the positive mass budget. The accumulated ice mass would accelerate a glacier to surge (Eisen et al., 2005; Kochtitzky et al., 2020), and the significant mass loss could prevent or postpone the surge in return (Dowdeswell et al., 1995). On a regional large scale, the relationship between mass balance and surge occurrence needs to be further analyzed. Our glacier elevation change maps of the period 2000-2010s are similar to that derived by Brun et al. (2017) and Shean et al. (2020). We found that, at the regional scale, the occurrence of surging glaciers is correlated with the regional glacier mass balance. The three subregions holding the largest clusters of surging glaciers, i.e., the Pamirs, Karakoram, and West Kunlun, are characterized by slightly negative or positive elevation changes, which is known as one part of the 'Pamir-Karakoram-West Kunlun' anomaly (Brun et al., 2017). Likewise, the subregions Central Tien Shan, Tibetan Interior Mountains, and East Kunlun Shan, which hold the moderate clusters of surging glaciers, have glacier mass loss rates much lower than the average rates of HMA. By contrast, subregions with severe glacier mass loss hold the lowest surging glacier ratio, such as the Dzhungarsky Alatau, Hengduan Shan, and Eastern Himalaya.

6.3 Comparison with previous surging glacier inventories

Guillet et al. (2022) presented a comprehensive surging glacier inventory of HMA for the period 2000-2018 from a multi-factor remote sensing approach. Prior to the comparison, we generated an inventory based on the RGI6.0, as Guillet et al. (2022) did. Guillet et al. (2022) identified 666 surging glaciers, and the area of surging glaciers occupies 19.5% of the total glacier area. We identified 890 surging glaciers (809 if represented by RGI6.0 polygons), and their area only occupies 16.59% of the total glacier area. We attributed the lower area ratio of surging glaciers to two reasons. First, in our inventory, the surging tributaries were separated from the non-surging trunks. Second, many outcrop rocks and shaded areas are excluded from the GAMDAM2 glacier areas (Sakai, 2019), which would lower our surging area ratio, but make the result more accurate. If we assign our identified surging glaciers to the RGI6.0 polygons without tributary separation, the surging area ratio would be larger (20.25%).

Within our inventory, 556 surging and 62 surge-like glaciers were also identified by Guillet et al. (2022), and the discrepancy of identifications mostly occurred on small glaciers. If only the period 2000-2020 was considered, 657 surging glaciers were identified by us, which is very close to that of Guillet et al. (665). For the period 1970s-2000, 151 surging and 101 surge-like glaciers that were not identified by Guillet et al. (2022). Overall, we have newly identified 253 surging and 248 surge-like glaciers. We owed the new findings to the longer observation period and multiple elevation change observations. However, 47 surging glaciers presented by Guillet et al. were missed in this study, and 62 surge-like glaciers in our new inventory were identified as surging glaciers by Guillet et al. (2022). We carefully checked the glaciers not included in our inventory but included in Guillet et al.'s inventory, as well as those included in our inventory but not included in Guillet et al.'s inventory, and this step helped us to find 21 more surging glaciers. We attribute this to the deficiency of using a single criterion, which could be aided by combining other features. Besides, the DEMs used in this study were suffering from data voids and incomplete spatial coverage, especially for the KH-9 DEM, which could result in a relatively conservative identification.

Multiple studies have identified surging glaciers in the Karakoram based on different data sources. For example, Bhambri et al. (2017) identified 221 surging and surge-like glaciers (counting tributaries of a glacier system as individual glaciers) based on glacier morphological changes detected from space-borne optical images acquired from 1972 to 2016, in-situ observations, and archive photos dating back to the 1840s. However, the boundary used by Bhambri et al. (2017) to define the extent of Karakoram is much smaller than that used in our inventory. A much smaller group of surging glaciers (88) was identified by Copland et al. (2011) based on a similar method and the data acquired between 1960 and 2013. Rankl et al. (2014) identified 101 surging glaciers in the Karakoram by detecting changes in glacier surface velocity and terminus position between 1976 and 2012. The results of Guillet et al. (2022) should be more reliable than previous ones because more criteria were used for identifying surging glaciers. Compared with previous inventories, our inventory includes more surging glaciers (354). Among the 223 surging glaciers in the Karakoram identified by Guillet et al. (2022), 203 were identified as surging glaciers, and 12 were identified as surge-like glaciers in this study, which means only 8 surging glaciers presented by Guillet et al. (2022) were not included in our inventory. The high coincidence between the two inventories indicates our surging glacier identification result is reliable. In total, we have newly identified 101 surging and 101 surge-like glaciers in this region.

Based on the method of glacier terminus change monitoring in Google Earth Engine, Vale et al. (2021) identified obvious terminus change of 137 surging glaciers. We found that 127 verified surging and 6 surge-like glaciers in our inventory were included in their inventory, i.e., only four glaciers were missed in this study. The possible reason for this gap is that the technique used by Vale et al. cannot identify the internal glacier surges that did not result in a terminus advance. Also, the inadequate quality and spatial resolution of satellite images could limit the performance of detecting changes in glacier terminus position.

In the Pamirs, Sevestre and Been (2015) identified 820 surge-type glaciers based on publications and reports, but Goerlich et al. (2020) reported only 186 surging glaciers based on observations of glacier flow velocity, elevation change, etc. We found that if Goerlich et al. (2020) applied the GAMDAM2 glacier polygons used in this study, the number of identified surging

glaciers would be 182. Among the 182 surging glaciers identified by Goerlich et al. (2020), 153 were identified as surging glaciers and 15 were identified as surge-like glaciers in our study. Although 14 surging glaciers are missed in this study, our inventory has contained other 94 surging and 44 surge-like glaciers. The main cause for the discrepancy is that the glacier elevation change observation before 2000 conducted by Goerlich et al. (2020) only covered a small part of the Western Pamir. In this region, our inventory shared 193 surging glaciers with Guillet et al.'s inventory, and 185 of them were identified during the period 2000-2020, which also manifests a high coincidence of the two results.

In the West Kunlun, Yasuda and Furuya (2015) reported 9 surging glaciers in the main range only, based on changes in glacier flow velocity and terminus position of 31 glaciers, and another 9 surging glaciers were found in the northwest part of the West Kunlun Shan by Chudley et al. (2019). A larger number (60) were found by Guillet et al. (2022). However, our inventory has even included more surging (82) and surge-like (47) glaciers in the West Kunlun Shan. During the period 2000-2020, we have identified 61 surging glaciers, which is very close to the number presented by Guillet et al. (2022). In Central Tien Shan, Mukherjee et al. (2017) identified 39 surge-type (including 9 surging and 13 very probable surging) glaciers through the analysis of changes in surface elevation and morphology from 1964 to 2014, whereas 79 (59 surging and 20 surge-like) were identified in our studies. The insufficient coverage of elevation change observation (only covering the west part of the Central Tien Shan) may be the main reason for the discrepancy in identification results. Guillet et al. (2022) identified 54 surging glaciers during 2000-2018, in which 36 were confirmed in our inventory.

7 Conclusions

This study presents a new inventory of surging glaciers across the entire HMA range, which was accomplished based on the glacier surface elevation changes derived from multiple elevation sources, by using the morphological changes from optical images as complements. In total, 890 surging and 336 probably or possibly surging glaciers were identified in the new inventory. Through the analysis of geometric parameters, we found that surging glaciers generally have a greater area, length, and elevation range than non-surging glaciers. However, the differences are smaller when taking the glacier size distribution into account. When considering glaciers of similar areas, the steeper ones are more likely to surge. Furthermore, by combining the region-wide glacier mass balance measurements, we found a similar distribution between the positive mass balance and the number of surging glaciers. Benefiting from the long period and wide coverage of surface elevation change observations, our study newly identified 253 surging and 248 surge-like glaciers in HMA than the previous inventory (Guillet et al., 2022). However, our inventory does not provide the surge duration period and the maximum flow velocity to describe the dynamic process of each glacier surge activity. Improvements should be made by combining multi-criteria identification methods. Considering the fact that glacier surges are more widespread than we thought, the inventory presented in this study still needs further replenishment.

8 Data and code availability

The presented inventory and corresponding multi-temporal elevation change results of identified surging glaciers are freely available at: https://doi.org/10.5281/zenodo.7590838 (Guo et al., 2022). The inventory is distributed in the format of GeoPackage (.gpkg) and ESRI shapefile (.shp), which is represented by outlines and manually defined center points of surging glaciers with geometric attributes. The glacier polygons of the inventory are compiled from the GAMDAM2 glacier inventory. In total, eight fields are integrated into the attributes table to describe the surging information of the corresponding glacier as mentioned in section 4.3. The description of each field in the attribute table is listed in Table 4. The DEM differencing results of the COP30 DEM – NASADEM, HMA DEM – NASADEM, and NASADEM – KH-9 DEM are compressed into individual zip files, respectively. The elevation change results of surging glaciers were divided into multi-temporal 1° × 1° tiled GeoTiff

grids. The metadata file is stored in a text file (README.txt), which contains the datasets description and details of the attribute information of the inventory.

The code used for elevation change estimation can be available at: https://github.com/TristanBlus/dem_coreg. This code was developed based on the *demcoreg* package (Shean et al., 2019).

Author contribution

J.L. and L.G. conceived this study and wrote the paper. L.G. developed the processing flow, complied the inventory, and drew the figures with support from J.L. A.D. generated the KH-9 DEM. A.D., Z.L., and X.L. helped with the results analysis and discussions, as well as manuscript editing. Z.L., J.L., and J.Z. provided funding acquisition. All authors have contributed and agreed to the published version of the manuscript.

Competing interest

The authors declare that they have no conflict of interest.

Acknowledgments

The authors express their gratitude to all institutions that provide us with the opensource dataset used in this study: the NASA DEM from LP DAAC (https://e4ftl01.cr.usgs.gov/MEASURES/NASADEM_HGT.001/), the Copernicus DEM from European Space Agency (ESA) (https://spacedata.copernicus.eu/web/cscda/cop-dem-faq), the HMA DEM processed by David Shean from National Snow and Ice Data Center (NSIDC) (https://nsidc.org/data/HMA_DEM8m_MOS/versions/1), and the Randolph Glacier Inventory Version 6.0 (http://www.glims.org/RGI/randolph.html). The authors also appreciate the valuable comments from Frank Paul and Guillet Gregoire.

Financial support

This work was supported by the Strategic Priority Research Program of Chinese Academy of Sciences (XDA20100101), the National Natural Science Fund for Distinguished Young Scholars (41925016), the Hunan Key Laboratory of Remote Sensing of Ecological Environment in Dongting Lake Area (No. 2021-010), the National Natural Science Foundation of China (41904006), the Fundamental Research Funds for the Central Universities of Central South University (2021zzts0265).

References

Abdel Jaber, W., Rott, H., Floricioiu, D., Wuite, J., and Miranda, N.: Heterogeneous spatial and temporal pattern of surface elevation change and mass balance of the Patagonian ice fields between 2000 and 2016, The Cryosphere, 13, 2511–2535, doi:10.5194/tc-13-2511-2019, 2019.

AIRBUS: Copernicus Digital Elevation Model Validation Report, AIRBUS Defence and Space GmbH, 2020.

An, B., Wang, W., Yang, W., Wu, G., Guo, Y., Zhu, H., Gao, Y., Bai, L., Zhang, F., Zeng, C., Wang, L., Zhou, J., Li, X., Li, J., Zhao, Z., Chen, Y., Liu, J., Li, J., Wang, Z., Chen, W., and Yao, T.: Process, mechanisms, and early warning of glacier collapse-induced river blocking disasters in the Yarlung Tsangpo Grand Canyon, southeastern Tibetan Plateau, Sci. Total Environ., 151652, doi:10.1016/j.scitotenv.2021.151652, 2021.

Barrand, N. E. and Murray, T.: Multivariate Controls on the Incidence of Glacier Surging in the Karakoram Himalaya, Arct. Antarct. Alp. Res., 38, 489–498, doi:10.1657/1523-0430(2006)38[489:MCOTIO]2.0.CO;2, 2006.

Beaud, F., Aati, S., Delaney, I., Adhikari, S., and Avouac, J.-P.: Generalized sliding law applied to the surge dynamics of Shisper Glacier and constrained by timeseries correlation of optical satellite images, Glaciers/Remote Sensing, doi:10.5194/tc-2021-96, 2021.

Benn, D. I., Fowler, A. C., Hewitt, I., and Sevestre, H.: A general theory of glacier surges, J. Glaciol., 65, 701–716, doi:10.1017/jog.2019.62, 2019.

Bhambri, R., Hewitt, K., Kawishwar, P., and Pratap, B.: Surge-type and surge-modified glaciers in the Karakoram, Sci. Rep., 7, doi:10.1038/s41598-017-15473-8, 2017.

Bhambri, R., Hewitt, K., Haritashya, U. K., Chand, P., Kumar, A., Verma, A., Tiwari, S. K., and Rai, S. K.: Characteristics of surge-type tributary glaciers, Karakoram, Geomorphology, 403, 108161, doi:10.1016/j.geomorph.2022.108161, 2022.

Bolch, T., Kulkarni, A., Kaab, A., Huggel, C., Paul, F., Cogley, J. G., Frey, H., Kargel, J. S., Fujita, K., Scheel, M., Bajracharya, S., and Stoffel, M.: The State and Fate of Himalayan Glaciers, Science, 336, 310–314, doi:10.1126/science.1215828, 2012.

Bolch, T., Pieczonka, T., Mukherjee, K., and Shea, J.: Brief communication: Glaciers in the Hunza catchment (Karakoram) have been nearly in balance since the 1970s, The Cryosphere, 11, 531–539, doi:10.5194/tc-11-531-2017, 2017.

Bolch, T., Shea, J. M., Liu, S., Azam, F. M., Gao, Y., Gruber, S., Immerzeel, W. W., Kulkarni, A., Li, H., Tahir, A. A., Zhang, G., and Zhang, Y.: Status and Change of the Cryosphere in the Extended Hindu Kush Himalaya Region, in: The Hindu Kush Himalaya Assessment, edited by: Wester, P., Mishra, A., Mukherji, A., and Shrestha, A. B., Springer International Publishing, Cham, 209–255, doi:10.1007/978-3-319-92288-1_7, 2019.

Brun, F., Berthier, E., Wagnon, P., Kääb, A., and Treichler, D.: A spatially resolved estimate of High Mountain Asia glacier mass balances from 2000 to 2016, Nat. Geosci., 10, 668–673, doi:10.1038/ngeo2999, 2017.

Chudley, T. R. and Willis, I. C.: Glacier surges in the north-west West Kunlun Shan inferred from 1972 to 2017 Landsat imagery, J. Glaciol., 65, 1–12, doi:10.1017/jog.2018.94, 2019.

Clarke, G. K. C.: Length, width and slope influences on glacier surging, J. Glaciol., 37, 236–246, doi:10.3189/S0022143000007255, 1991.

Clarke, G. K. C., Schmok, J. P., Ommanney, C. S. L., and Collins, S. G.: Characteristics of surge-type glaciers, J. Geophys. Res. Solid Earth, 91, 7165–7180, doi:10.1029/JB091iB07p07165, 1986.

Cogley, J. G., Arendt, A. A., Bauder, A., Braithwaite, R. J., Hock, R., J, B., R., Jansson, P., Kaser, G., Moller, M., Nicholson, L., Rasmussen, L. A., and Zemp, M.: Glossary of glacier mass balance and related terms, IACS Contribution No.2, UNESCO, Paris, 2011.

Copland, L., Sylvestre, T., Bishop, M. P., Shroder, J. F., Seong, Y. B., Owen, L. A., Bush, A., and Kamp, U.: Expanded and Recently Increased Glacier Surging in the Karakoram, Arct. Antarct. Alp. Res., 43, 503–516, 2011.

Crippen, R., Buckley, S., Agram, P., Belz, E., Gurrola, E., Hensley, S., Kobrick, M., Lavalle, M., Martin, J., Neumann, M., Nguyen, Q., Rosen, P., Shimada, J., Simard, M., and Tung, W.: NASADEM global elevation model: methods and progress, ISPRS - Int. Arch. Photogramm. Remote Sens. Spat. Inf. Sci., XLI-B4, 125–128, doi:10.5194/isprsarchives-XLI-B4-125-2016, 2016.

Dehecq, A., Gardner, A. S., Alexandrov, O., McMichael, S., Hugonnet, R., Shean, D., and Marty, M.: Automated Processing of Declassified KH-9 Hexagon Satellite Images for Global Elevation Change Analysis Since the 1970s, Front. Earth Sci., 8, 566802, doi:10.3389/feart.2020.566802, 2020.

Dowdeswell, J. A., Hodgkins, R., Nuttall, A.-M., Hagen, J. O., and Hamilton, G. S.: Mass balance change as a control on the frequency and occurrence of glacier surges in Svalbard, Norwegian High Arctic, Geophys. Res. Lett., 22, 2909–2912, doi:10.1029/95GL02821, 1995.

Eisen, O., Harrison, W. D., Raymond, C. F., Echelmeyer, K. A., Bender, G. A., and Gorda, J. L. D.: Variegated Glacier, Alaska, USA: a century of surges, J. Glaciol., 51, 399–406, doi:10.3189/172756505781829250, 2005.

Fan, Y., Ke, C.-Q., Zhou, X., Shen, X., Yu, X., and Lhakpa, D.: Glacier mass-balance estimates over High Mountain Asia from 2000 to 2021 based on ICESat-2 and NASADEM, J. Glaciol., 1–13, doi:10.1017/jog.2022.78, 2022.

Farinotti, D., Immerzeel, W. W., Kok, R., Quincey, D. J., and Dehecq, A.: Manifestations and mechanisms of the Karakoram glacier Anomaly, Nat. Geosci., 13, 8–16, doi:10.1038/s41561-019-0513-5, 2020.

Farnsworth, W. R., Ingólfsson, Ó., Retelle, M., and Schomacker, A.: Over 400 previously undocumented Svalbard surge-type glaciers identified, Geomorphology, 264, 52–60, doi:10.1016/j.geomorph.2016.03.025, 2016.

Farr, T. G., Rosen, P. A., Caro, E., Crippen, R., Duren, R., Hensley, S., Kobrick, M., Paller, M., Rodriguez, E., Roth, L., Seal, D., Shaffer, S., Shimada, J., Umland, J., Werner, M., Oskin, M., Burbank, D., and Alsdorf, D.: The Shuttle Radar Topography Mission, Rev. Geophys., 45, RG2004, doi:10.1029/2005RG000183, 2007.

Fowler, A. C.: A theory of glacier surges, J. Geophys. Res., 92, 9111, doi:10.1029/JB092iB09p09111, 1987.

Fowler, A. C., Murray, T., and Ng, F. S. L.: Thermally controlled glacier surging, J. Glaciol., 47, 527–538, doi:10.3189/172756501781831792, 2001.

Gardelle, J., Berthier, E., Arnaud, Y., and Kääb, A.: Region-wide glacier mass balances over the Pamir-Karakoram-Himalaya during 1999–2011, Cryosphere Discuss., 7, 975–1028, doi:10.5194/tcd-7-975-2013, 2013.

Goerlich, F., Bolch, T., and Paul, F.: More dynamic than expected: an updated survey of surging glaciers in the Pamir, Earth Syst. Sci. Data, 12, 3161–3176, doi:10.5194/essd-12-3161-2020, 2020.

Guillet, G., King, O., Lv, M., Ghuffar, S., Benn, D., Quincey, D., and Bolch, T.: A regionally resolved inventory of High Mountain Asia surge-type glaciers, derived from a multi-factor remote sensing approach, The Cryosphere, 16, 603–623, doi:10.5194/tc-16-603-2022, 2022.

Guth, P. L. and Geoffroy, T. M.: LiDAR point cloud and ICESat-2 evaluation of 1 second global digital elevation models: Copernicus wins, Trans. GIS, 25, 2245–2261, doi:10.1111/tgis.12825, 2021.

Hewitt, K.: The Karakoram Anomaly? Glacier Expansion and the 'Elevation Effect,' Karakoram Himalaya, Mt. Res. Dev., 25, 332–340, doi:10.1659/0276-4741(2005)025[0332:TKAGEA]2.0.CO;2, 2005.

Hewitt, K.: Tributary glacier surges: an exceptional concentration at Panmah Glacier, Karakoram Himalaya, J. Glaciol., 53, 181–188, doi:10.3189/172756507782202829, 2007.

Höhle, J. and Höhle, M.: Accuracy assessment of digital elevation models by means of robust statistical methods, ISPRS J. Photogramm. Remote Sens., 64, 398–406, doi:10.1016/j.isprsjprs.2009.02.003, 2009.

Holzer, N., Vijay, S., Yao, T., Xu, B., Buchroithner, M., and Bolch, T.: Four decades of glacier variations at Muztagh Ata (eastern Pamir): a multi-sensor study including Hexagon KH-9 and Pléiades data, The Cryosphere, 9, 2071–2088, doi:10.5194/tc-9-2071-2015, 2015.

Hugonnet, R., McNabb, R., Berthier, E., Menounos, B., Nuth, C., Girod, L., Farinotti, D., Huss, M., Dussaillant, I., Brun, F., and Kääb, A.: Accelerated global glacier mass loss in the early twenty-first century, Nature, 592, 726–731, doi:10.1038/s41586-021-03436-z, 2021.

Jacquemart, M. and Cicoira, A.: Hazardous Glacier Instabilities: Ice Avalanches, Sudden Large-Volume Detachments of Low-Angle Mountain Glaciers, and Glacier Surges, in: Treatise on Geomorphology, Elsevier, 330–345, doi:10.1016/B978-0-12-818234-5.00188-7, 2022.

Jiskoot, H.: Glacier Surging, in: Encyclopedia of Snow, Ice and Glaciers, edited by: Singh, V. P., Singh, P., and Haritashya, U. K., Springer Netherlands, Dordrecht, 415–428, doi:10.1007/978-90-481-2642-2_559, 2011.

Jiskoot, H., Murray, T., and Boyle, P.: Controls on the distribution of surge-type glaciers in Svalbard, J. Glaciol., 46, 412–422, doi:10.3189/172756500781833115, 2000.

Kääb, A., Leinss, S., Gilbert, A., Bühler, Y., Gascoin, S., Evans, S. G., Bartelt, P., Berthier, E., Brun, F., Chao, W.-A., Farinotti, D., Gimbert, F., Guo, W., Huggel, C., Kargel, J. S., Leonard, G. J., Tian, L., Treichler, D., and Yao, T.: Massive collapse of

two glaciers in western Tibet in 2016 after surge-like instability, Nat. Geosci., 11, 114–120, doi:10.1038/s41561-017-0039-7, 2018.

Kääb, A., Jacquemart, M., Gilbert, A., Leinss, S., Girod, L., Huggel, C., Falaschi, D., Ugalde, F., Petrakov, D., Chernomorets, S., Dokukin, M., Paul, F., Gascoin, S., Berthier, E., and Kargel, J. S.: Sudden large-volume detachments of low-angle mountain glaciers – more frequent than thought?, The Cryosphere, 15, 1751–1785, doi:10.5194/tc-15-1751-2021, 2021.

Kamb, B.: Glacier surge mechanism based on linked cavity configuration of the basal water conduit system, J. Geophys. Res., 92, 9083, doi:10.1029/JB092iB09p09083, 1987.

Kochtitzky, W., Winski, D., McConnell, E., Kreutz, K., Campbell, S., Enderlin, E. M., Copland, L., Williamson, S., Main, B., and Jiskoot, H.: Climate and surging of Donjek Glacier, Yukon, Canada, Arct. Antarct. Alp. Res., 52, 264–280, doi:10.1080/15230430.2020.1744397, 2020.

Li, J., Li, Z., Zhu, J., Li, X., Xu, B., Wang, Q., Huang, C., and Hu, J.: Early 21st century glacier thickness changes in the Central Tien Shan, Remote Sens. Environ., 192, 12–29, doi:10.1016/j.rse.2017.02.003, 2017.

Lv, M., Guo, H., Lu, X., Liu, G., Yan, S., Ruan, Z., Ding, Y., and Quincey, D. J.: Characterizing the behaviour of surge- and non-surge-type glaciers in the Kingata Mountains, eastern Pamir, from 1999 to 2016, The Cryosphere, 13, 219–236, doi:10.5194/tc-13-219-2019, 2019.

Lv, M., Guo, H., Yan, J., Wu, K., Liu, G., Lu, X., Ruan, Z., and Yan, S.: Distinguishing Glaciers between Surging and Advancing by Remote Sensing: A Case Study in the Eastern Karakoram, Remote Sens., 12, 2297, doi:10.3390/rs12142297, 2020.

Maurer, J. M., Schaefer, J. M., Rupper, S., and Corley, A.: Acceleration of ice loss across the Himalayas over the past 40 years, Sci. Adv., 5, eaav7266, doi:10.1126/sciadv.aav7266, 2019.

Maussion, F., Scherer, D., Mölg, T., Collier, E., Curio, J., and Finkelnburg, R.: Precipitation Seasonality and Variability over the Tibetan Plateau as Resolved by the High Asia Reanalysis, J. Clim., 27, 1910–1927, doi:10.1175/JCLI-D-13-00282.1, 2014.

Maussion, F., Butenko, A., Champollion, N., Dusch, M., Eis, J., Fourteau, K., Gregor, P., Jarosch, A. H., Landmann, J., Oesterle, F., Recinos, B., Rothenpieler, T., Vlug, A., Wild, C. T., and Marzeion, B.: The Open Global Glacier Model (OGGM) v1.1, Geosci. Model Dev., 12, 909–931, doi:10.5194/gmd-12-909-2019, 2019.

Muhammad, S., Li, J., Steiner, J. F., Shrestha, F., Shah, G. M., Berthier, E., Guo, L., Wu, L., and Tian, L.: A holistic view of Shisper Glacier surge and outburst floods: from physical processes to downstream impacts, Geomat. Nat. Hazards Risk, 12, 2755–2775, doi:10.1080/19475705.2021.1975833, 2021.

Mukherjee, K., Bolch, T., Goerlich, F., Kutuzov, S., Osmonov, A., Pieczonka, T., and Shesterova, I.: Surge-Type Glaciers in the Tien Shan (Central Asia), Arct. Antarct. Alp. Res., 49, 147–171, doi:10.1657/AAAR0016-021, 2017.

Murray, T., Strozzi, T., Luckman, A., Jiskoot, H., and Christakos, P.: Is there a single surge mechanism? Contrasts in dynamics between glacier surges in Svalbard and other regions: IS THERE A SINGLE SURGE MECHANISM?, J. Geophys. Res. Solid Earth, 108, doi:10.1029/2002JB001906, 2003.

Nuimura, T., Sakai, A., Taniguchi, K., Nagai, H., Lamsal, D., Tsutaki, S., Kozawa, A., Hoshina, Y., Takenaka, S., Omiya, S., Tsunematsu, K., Tshering, P., and Fujita, K.: The GAMDAM glacier inventory: a quality-controlled inventory of Asian glaciers, The Cryosphere, 9, 849–864, doi:10.5194/tc-9-849-2015, 2015.

Nuth, C. and Kääb, A.: Co-registration and bias corrections of satellite elevation data sets for quantifying glacier thickness change, The Cryosphere, 5, 271–290, doi:10.5194/tc-5-271-2011, 2011.

Paul, F.: Revealing glacier flow and surge dynamics from animated satellite image sequences: examples from the Karakoram, The Cryosphere, 9, 2201–2214, doi:10.5194/tc-9-2201-2015, 2015.

Paul, F.: Repeat Glacier Collapses and Surges in the Amney Machen Mountain Range, Tibet, Possibly Triggered by a Developing Rock-Slope Instability, Remote Sens., 11, 708, doi:10.3390/rs11060708, 2019.

Purinton, B. and Bookhagen, B.: Beyond Vertical Point Accuracy: Assessing Inter-pixel Consistency in 30 m Global DEMs for the Arid Central Andes, Front. Earth Sci., 9, 758606, doi:10.3389/feart.2021.758606, 2021.

Quincey, D. J., Braun, M., Glasser, N. F., Bishop, M. P., Hewitt, K., and Luckman, A.: Karakoram glacier surge dynamics, Geophys. Res. Lett., 38, L18504, doi:10.1029/2011GL049004, 2011.

Rankl, M., Kienholz, C., and Braun, M.: Glacier changes in the Karakoram region mapped by multimission satellite imagery, The Cryosphere, 8, 977–989, doi:10.5194/tc-8-977-2014, 2014.

Round, V., Leinss, S., Huss, M., Haemmig, C., and Hajnsek, I.: Surge dynamics and lake outbursts of Kyagar Glacier, Karakoram, The Cryosphere, 11, 723–739, doi:10.5194/tc-11-723-2017, 2017.

Sakai, A.: Brief communication: Updated GAMDAM glacier inventory over high-mountain Asia, The Cryosphere, 13, 2043–2049, doi:10.5194/tc-13-2043-2019, 2019.

Sevestre, H. and Benn, D. I.: Climatic and geometric controls on the global distribution of surge-type glaciers: implications for a unifying model of surging, J. Glaciol., 61, 646–662, doi:10.3189/2015JoG14J136, 2015.

Shean, D., Shashank Bhushan, Lilien, D., and Meyer, J.: dshean/demcoreg: Zenodo DOI release, doi:10.5281/ZENODO.3243481, 2019.

Shean, D. E., Alexandrov, O., Moratto, Z. M., Smith, B. E., Joughin, I. R., Porter, C., and Morin, P.: An automated, open-source pipeline for mass production of digital elevation models (DEMs) from very-high-resolution commercial stereo satellite imagery, ISPRS J. Photogramm. Remote Sens., 116, 101–117, doi:10.1016/j.isprsjprs.2016.03.012, 2016.

Shean, D. E., Bhushan, S., Montesano, P., Rounce, D. R., Arendt, A., and Osmanoglu, B.: A Systematic, Regional Assessment of High Mountain Asia Glacier Mass Balance, Front. Earth Sci., 7, 363, doi:10.3389/feart.2019.00363, 2020.

Steiner, J. F., Kraaijenbrink, P. D. A., Jiduc, S. G., and Immerzeel, W. W.: Brief communication: The Khurdopin glacier surge revisited – extreme flow velocities and formation of a dammed lake in 2017, The Cryosphere, 12, 95–101, doi:10.5194/tc-12-95-2018, 2018.

Surazakov, A. and Aizen, V.: Positional Accuracy Evaluation of Declassified Hexagon KH-9 Mapping Camera Imagery, Photogramm. Eng. Remote Sens., 76, 603–608, doi:10.14358/PERS.76.5.603, 2010.

Thøgersen, K., Gilbert, A., Schuler, T. V., and Malthe-Sørenssen, A.: Rate-and-state friction explains glacier surge propagation, Nat. Commun., 10, 2823, doi:10.1038/s41467-019-10506-4, 2019.

Vale, A. B., Arnold, N. S., Rees, W. G., and Lea, J. M.: Remote Detection of Surge-Related Glacier Terminus Change across High Mountain Asia, Remote Sens., 13, 1309, doi:10.3390/rs13071309, 2021.

Van Wyk de Vries, M., Wickert, A. D., MacGregor, K. R., Rada, C., and Willis, M. J.: Atypical landslide induces speedup, advance, and long-term slowdown of a tidewater glacier, Geology, doi:10.1130/G49854.1, 2022.

Yamazaki, D., Ikeshima, D., Tawatari, R., Yamaguchi, T., O'Loughlin, F., Neal, J. C., Sampson, C. C., Kanae, S., and Bates, P. D.: A high-accuracy map of global terrain elevations, Geophys. Res. Lett., 44, 5844–5853, doi:10.1002/2017GL072874, 2017.

Yasuda, T. and Furuya, M.: Dynamics of surge-type glaciers in West Kunlun Shan, Northwestern Tibet, J. Geophys. Res. Earth Surf., 120, 2393–2405, doi:10.1002/2015JF003511, 2015.

Zhou, S., Yao, X., Zhang, D., Zhang, Y., Liu, S., and Min, Y.: Remote Sensing Monitoring of Advancing and Surging Glaciers in the Tien Shan, 1990–2019, Remote Sens., 13, 1973, doi:10.3390/rs13101973, 2021.

Zhou, Y., Li, Z., and Li, J.: Slight glacier mass loss in the Karakoram region during the 1970s to 2000 revealed by KH-9 images and SRTM DEM, J. Glaciol., 63, 331–342, doi:10.1017/jog.2016.142, 2017.

Zhou, Y., Li, Z., Li, J., Zhao, R., and Ding, X.: Glacier mass balance in the Qinghai–Tibet Plateau and its surroundings from the mid-1970s to 2000 based on Hexagon KH-9 and SRTM DEMs, Remote Sens. Environ., 210, 96–112, doi:10.1016/j.rse.2018.03.020, 2018.

Tables and Figures

Table 1: Surging glacier identification results

Glacier changes	Identification class			Total
	I	II	III	
2000-2020 elevation change	719	157	169	1045
1970s-2000 elevation change	507	156	57	720
1986-2021 terminus advance	247	397	-	645
1986-2021 looped moraine	112	31	-	144
1986-2021 medial moraine	69	29	-	108
Final identified surging glaciers	890 (verified)	208 (probable)	128 (possible)	1226

Table 2: Results of surging glacier identification in 22 subregions of HMA. Only glaciers larger than 0.4 km^2 were considered in the glacier number related values.

HiMAP regions	Glacier Number				Glacier Area			
	Surging	Surge-like	Total	Ratio (%)	Surging	Surge-like	Total	Ratio (%)
Karakoram	354	128	4121	8.59	7936.12	1329.40	20103.68	39.48
Western Pamir	188	48	3058	6.15	2232.52	289.597	8172.64	27.32
Western Kunlun Shan	82	47	2508	3.27	2580.21	589.17	8466.12	30.48
Central Tien Shan	59	20	2248	2.62	881.61	305.47	6816.95	12.93
Eastern Pamir	56	16	1148	4.88	796.35	79.12	2746.47	29.00
Tanggula Shan	22	4	697	3.16	441.94	41.71	1937.39	22.81
Tibetan Interior Mountains	22	12	1471	1.50	286.29	140.22	3933.48	7.28
Northern Western Tien Shan	21	6	1374	1.53	116.27	81.09	2502.60	4.65
Central Himalaya	17	21	3433	0.50	164.12	185.07	9928.72	1.65
Eastern Kunlun Shan	16	7	1191	1.34	458.11	55.38	2960.26	15.48
Nyainqentanglha	10	5	2916	0.34	119.53	184.79	7216.62	1.66
Eastern Hindu Kush	9	5	1279	0.70	178.18	77.19	3055.80	5.83
Western Himalaya	9	4	3659	0.25	110.22	69.41	8619.19	1.28
Eastern Himalaya	6	0	1334	0.45	94	0	3371.89	2.79
Pamir Alay	5	0	991	0.50	35.72	0	1957.94	1.82
Qilian Shan	4	6	851	0.47	35.99	26.40	1627.94	2.21
Eastern Tibetan Mountains	3	2	156	1.92	36.33	3.85	341.46	10.64
Altun Shan	2	3	156	1.28	4.13	3.17	294.95	1.40
Eastern Tien Shan	2	1	1243	0.16	12.03	2.59	2440.11	0.49
Hengduan Shan	2	0	700	0.29	26.22	0	1335.39	1.96
Gangdise Mountains	1	0	768	0.13	10.52	0	1339.54	0.79
Dzhungarsky Alatau	0	1	407	0	0	10.98	648.61	0
Total	890	336	35709	2.49	16556.42	3474.60	99817.72	16.59

* The value of ratio only considered the number and area of surging glaciers.

Table 3: The number and area ratios of surging glaciers in all glaciers for different area classes.

Area Class	Total		Surging Glacier		Ratio (%)	
	Count	Area (km^2)	Count	Area (km^2)	Count	Area
0.4-1	19428	12215.4	28	20.8	0.14	0.17
1-3	10983	18305.7	169	345.0	1.54	1.88
3-5	2404	9229.4	141	560.3	5.87	6.07

5-10	1650	11370.1	195	1416.4	11.82	12.46
10-30	946	15048.9	227	3861.2	24.00	25.66
30-50	161	5979.1	56	2036.5	34.78	34.06
50-100	92	6337.4	48	3329.2	52.17	52.53
100-300	39	6191.4	24	3651.5	61.54	58.98
>300	6	3466.3	2	1335.6	33.33	38.53

741

742 **Table 4: Attribute information in the present surging glacier inventory.**

Attribute	Description	Attribute	Description
Glac_ID	Glacier identifier composed by Lat/Lon	Surge_20	Surge identified in 2000-2020 by dH
Area	Glacier area (km^2)	Surge_70s	Surge identified in 1970s-2000 by dH
Zmin	Minimum elevation of the glacier (m a.s.l)	Delta_T	Identified class of glacier terminus advance
Zmax	Maximum elevation of the glacier (m a.s.l)	Loop_M	Identified class of looped moraine change
Zmed	Median elevation of the glacier (m a.s.l)	Medial_M	Identified class of medial moraine change
Slope	Mean glacier surface slope (°)	False_signal	False positive signal of identification
Aspect	Mean glacier aspect/orientation (°)	Trib_surge	If the glacier has/is surging tributary
MaxL	Maximum length of glacier flow line (m)	Surge_class	Final surge identification during 1970s-2020
HiMAP_region	HMA subregion that the glacier belongs to		

743

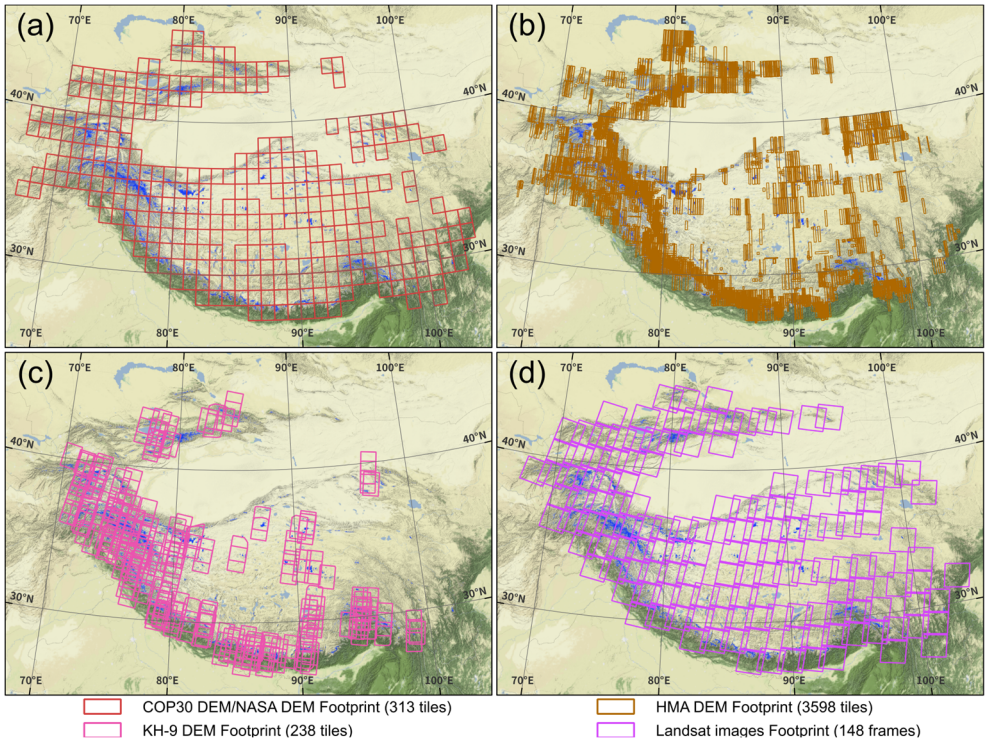

744

745 **Figure 1: Footprints of (a) the COP30/NASA DEMs, (b) the HMA DEMs, (c) the KH-9 DEMs, and (d) Landsat imageries that were**
746 **utilized in this study. The background is rendered from the ESRI World Physical base map (Source: US National Park Service).**

747

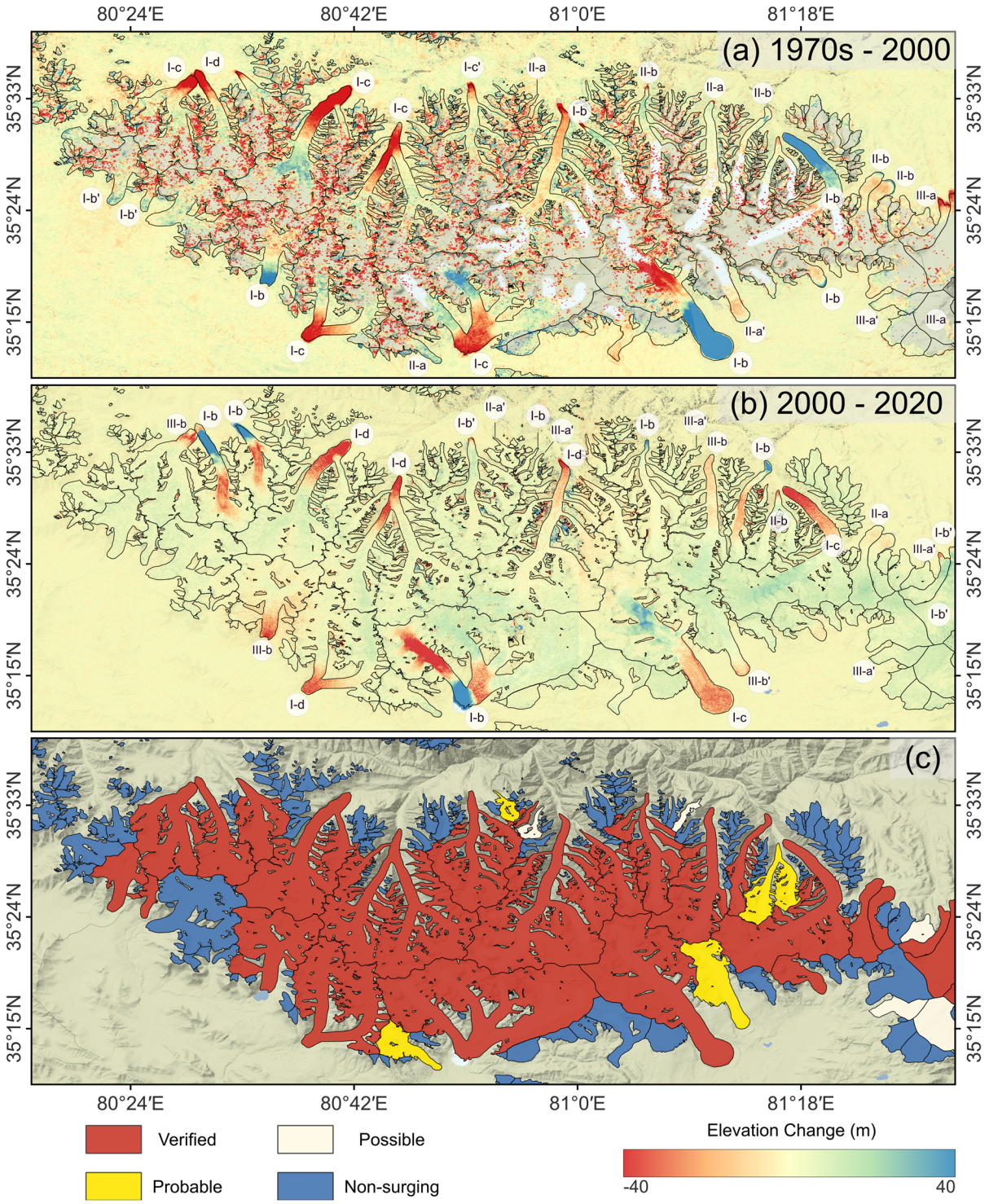

748

749 **Figure 2: An example of derived elevation change maps during (a) 1970s-2000, (b) 2000-2020, and (c) the surging glacier**
750 **identification results. Black curves are glacier outlines. The labels in panels (a) and (b) represent the identified classes based on the**
751 **elevation change patterns (the criteria of identification is elaborated in section 4.2.1). The subscript '' in the labels indicates that**
752 **the surging glacier is identified by combining other elevation change maps. The background is the shaded relief of the COP30 DEM**
753 **(Source: ESA). The area is in the main massif of Western Kunlun Shan.**

754

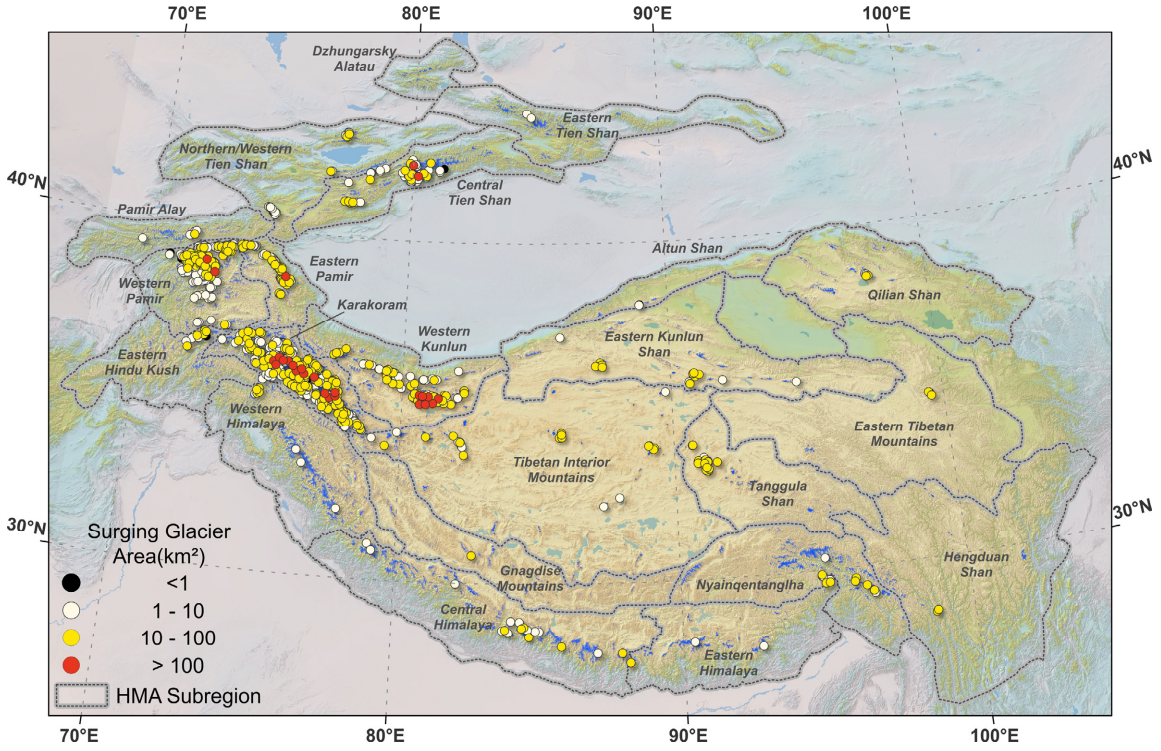

755

756 **Figure 3: Overview of the distribution of identified surging glaciers in 22 subregions of HMA. The background is the shaded relief**
757 **of SRTM DEM (Source: USGS).**

758

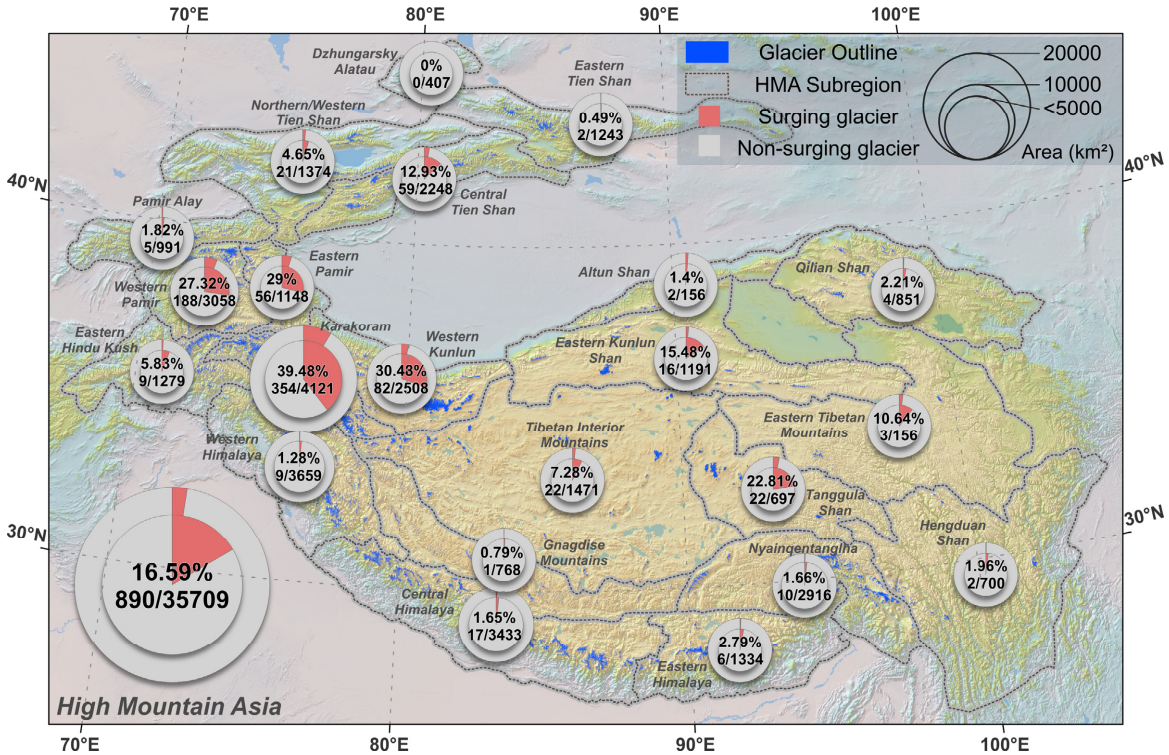

759

760 **Figure 4: Distribution of surging glaciers in the 22 subregions of HMA. The double-level pie chart represents the ratios of surging**
761 **glacier number and area in each subregion. The inner pie denotes the area ratio labeled by a percentage, and the outer pie denotes**
762 **the number ratio labeled by a fraction (only glaciers larger than 0.4 km^2 are considered). The background is the shaded relief of**
763 **SRTM DEM (Source: USGS).**

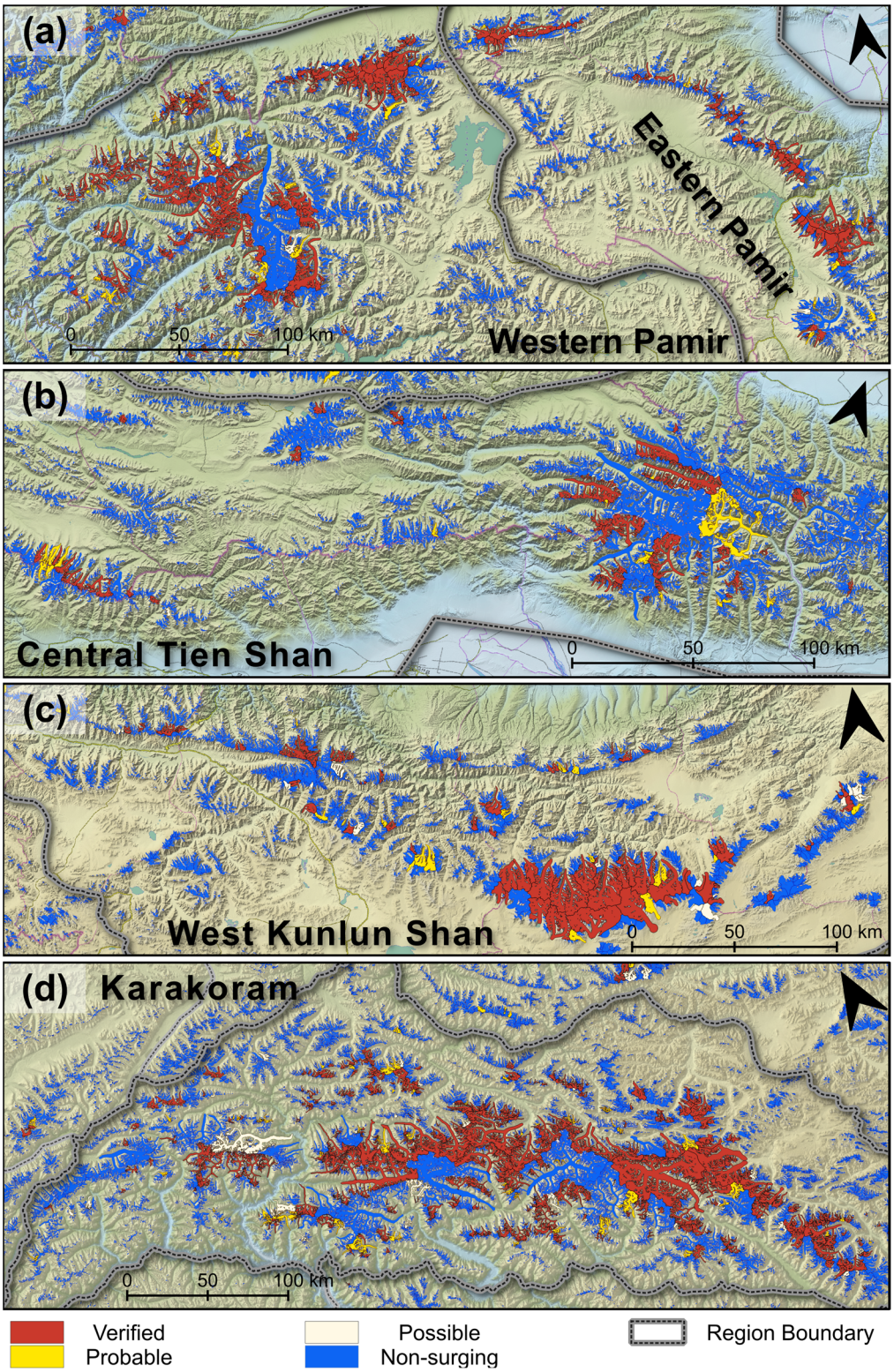

Figure 5: Results of surging glacier identification in (a) the Pamirs, (b) Central Tien Shan, (c) West Kunlun Shan, and (d) Karakoram. The background is the shaded relief of SRTM DEM (Source: USGS).

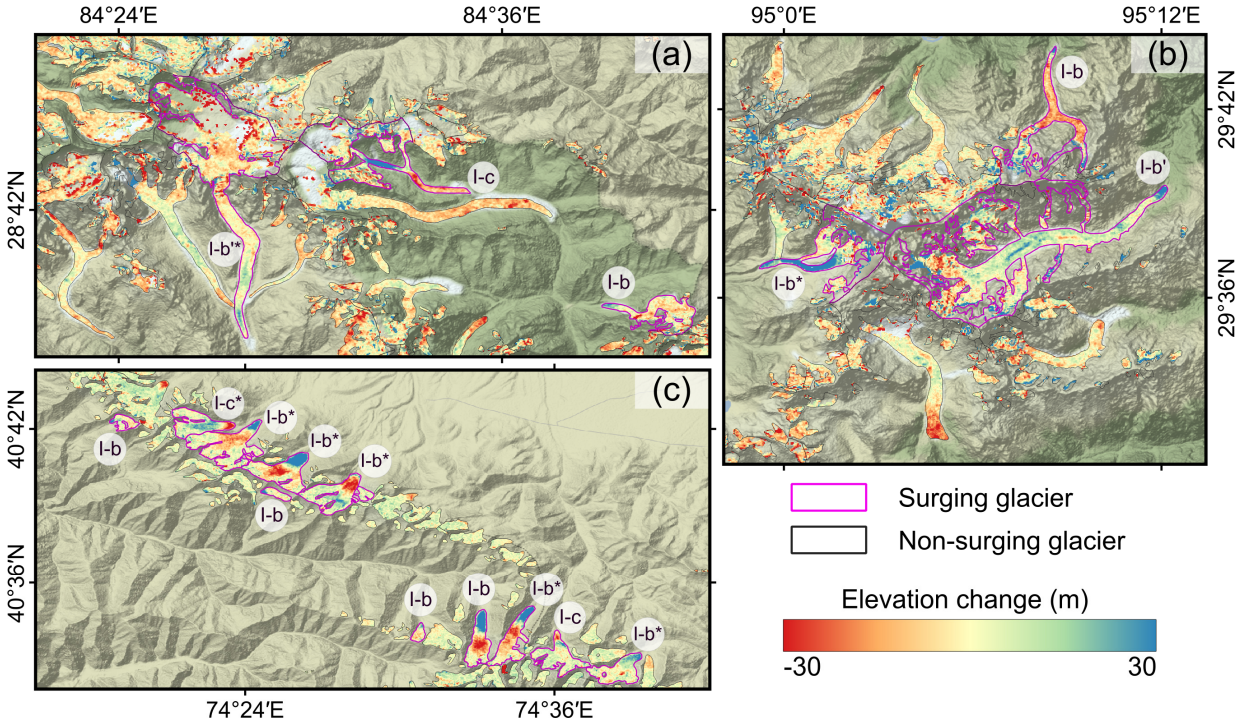

Figure 6: Elevation change map of identified surging glaciers samples in (a) Central Himalaya (1970s-2000), (b) Nyainqentanglha (1970s-2000), and (c) Northern Western Tien Shan (2000-2020). The labels in panels (a) and (b) represent the identified classes based on the elevation change pattern. The subscripts '*' and '' indicate that the identified class of the glacier is determined by combining morphological changes, and other elevation change maps, respectively. The background is the shaded relief of SRTM DEM (Source: USGS).

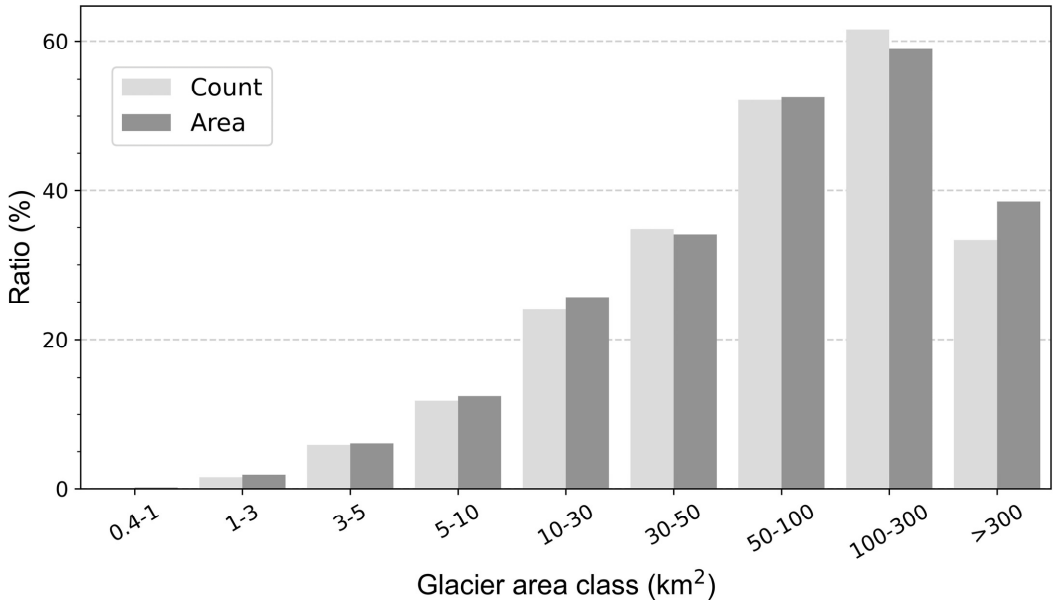

Figure 7: Illustration of the number and area ratios of surging glaciers for different area classes.

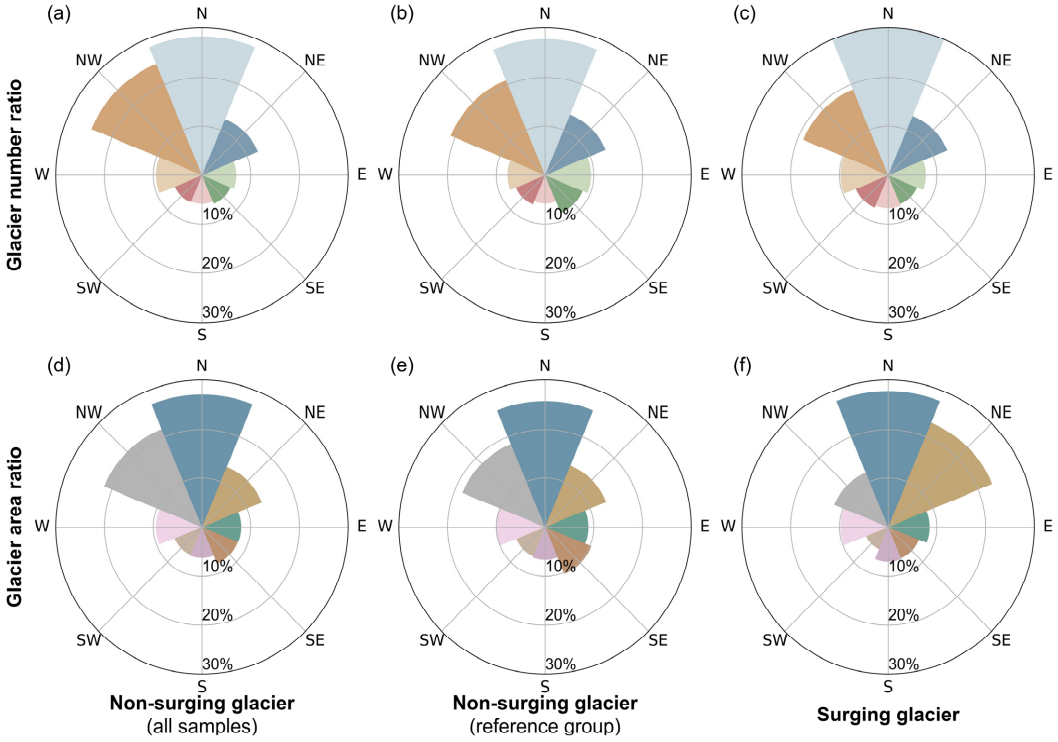

778

779 **Figure 8: The distribution of glacier number and area in eight aspect sectors. Left column (a) and (d): distribution of glacier number**
780 **and area ratio for non-surging glaciers; central column (b) and (e): distribution of glacier number and area ratio for non-surging**
781 **glaciers in the reference group; right column (c) and (f): distribution of glacier number and area ratio for all surging glaciers.**
782 **Glaciers smaller than 0.4 km^2 were excluded from the non-surging glacier class.**

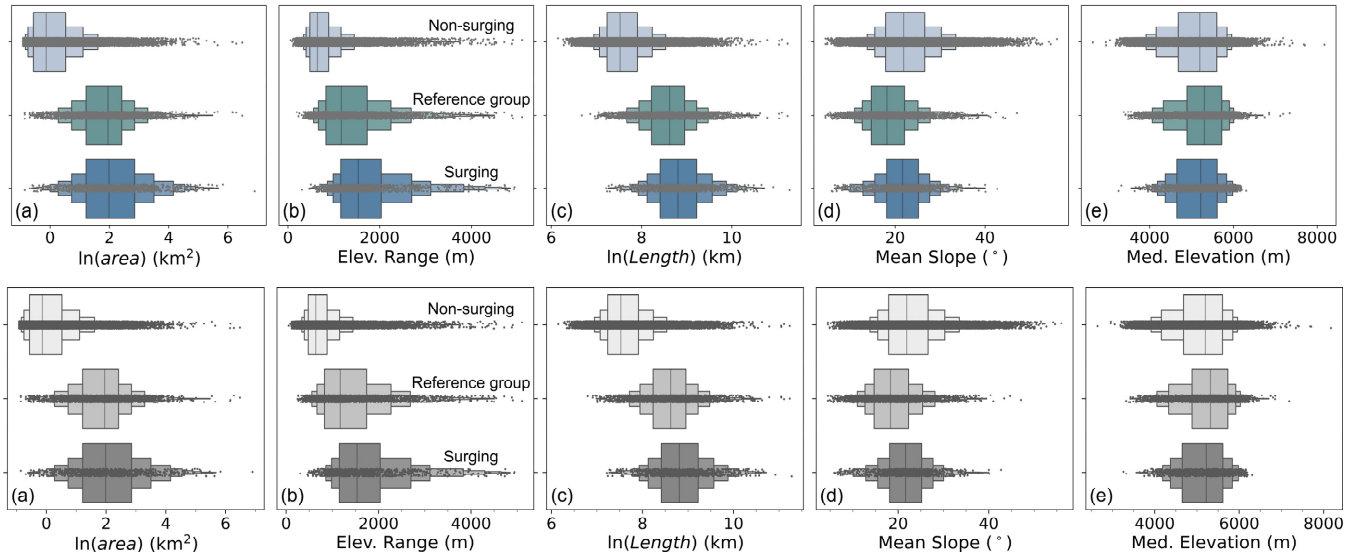

783

784

785 **Figure 9: The comparison between the boxplots of geometric properties of non-surging glaciers (top), non-surging glaciers in the**
786 **reference group (center), and surging glaciers (bottom). (a) Natural logarithm of area, (b) elevation range, (c) Natural logarithm of**
787 **length, (d) Mean surface slope, (e) Median elevation. Glaciers smaller than 0.4 km^2 were excluded from the non-surging glacier class.**

788

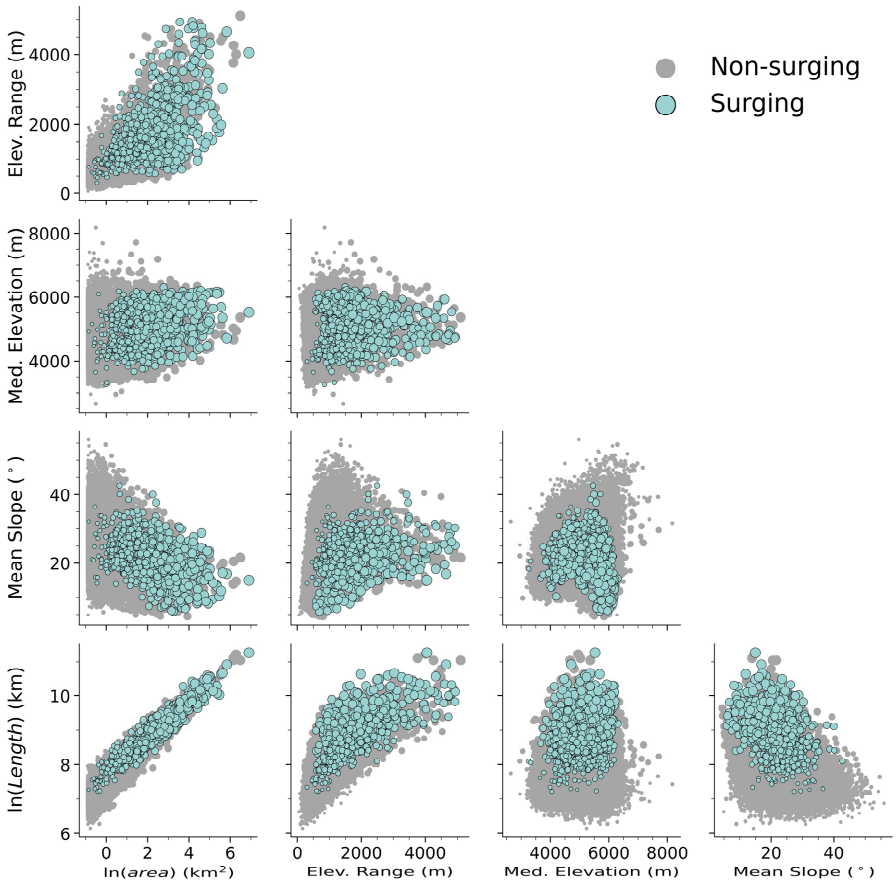

789

790 **Figure 10: Bivariate scatterplots of geometric properties of non-surging and surging glaciers. The larger dots represent larger**
791 **glaciers. Glaciers smaller than 0.4 km² were excluded in the non-surging glacier class.**

792

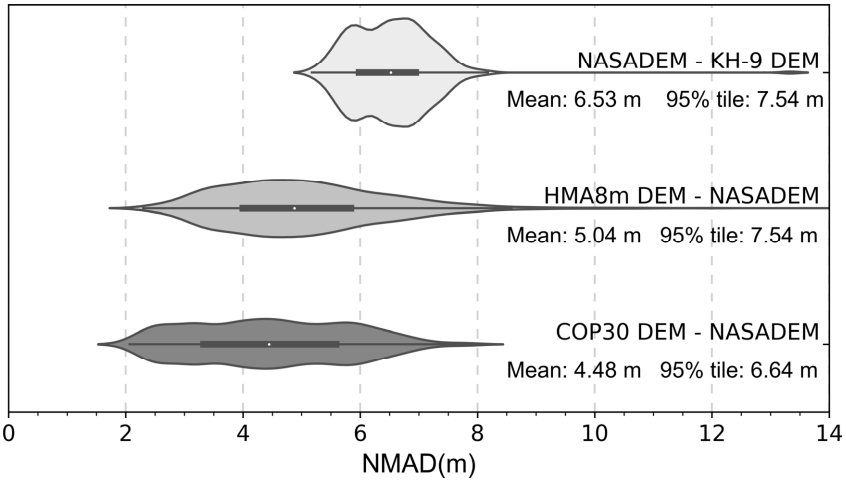

793

794 **Figure 11: The distribution of NMAD of elevation change observations in stable areas of all DEM differencing tiles. In each category,**
795 **the shaded area denotes the density distribution of the NMAD of all DEM differencing tiles. The white dot denotes the median in**
796 **each group. The thick line represents the interquartile range (IQR, i.e., 75th percentile-25th percentile) in each group. The thin line**
797 **represents the range between the minimum value (25th percentile - 1.5IQR) and the maximum value (75th percentile + 1.5IQR).**